JACS
JOURNAL OF THE AMERICAN CHEMICAL SOCIETY
Article
pubs.acs.org/JACS

The Influence of Anionic Ligands on Stereoisomerism of Ru Carbenes and Their Importance to Efficiency and Selectivity of Catalytic Olefin Metathesis Reactions

Sebastian Torker,[‡] R. Kashif M. Khan,[‡] and Amir H. Hoveyda*

Department of Chemistry, Merkert Chemistry Center, Boston College , Chestnut Hill, Massachusetts 02467, United States

Supporting Information

ABSTRACT: Investigations detailed herein provide insight regarding the mechanism of stereochemical inversion of stereogenic-at-Ru carbene complexes through a nonolefin metathesis-based polytopal rearrangement pathway. Computational analyses (DFT) reveal that there are two key factors that generate sufficient energy barriers that are responsible for the possibility of isolation and characterization of high-energy, but kinetically stable, intermediates: (1) donor−donor interactions that involve the anionic ligands and the strongly electron donating carbene groups and (2) dipolar effects arising from the syn relationship between the anionic groups (iodide and phenoxide). We demonstrate that a Brønsted acid lowers barriers to facilitate isomerization, and that the positive influence of a proton source is the result of its ability to diminish the repulsive electronic interactions originating from the anionic ligands. The implications of the present studies regarding a more sophisticated knowledge of the role of anionic units on the efficiency of Ru-catalyzed olefin metathesis reactions are discussed. The electronic basis for the increased facility with which allylic alcohols participate in olefin metathesis processes will be presented as well. Finally, we illustrate how a better understanding of the role of anionic ligands has served as the basis for successful design of Ru-based *Z*-selective catalysts for alkene metathesis.

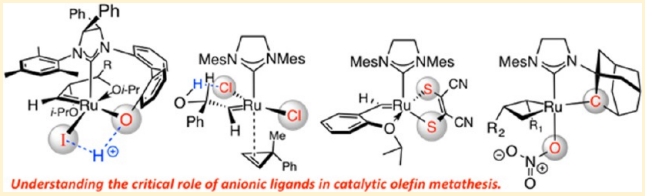

INTRODUCTION

Catalytic olefin metathesis (OM) has transformed the manner in which organic molecules of many shapes and sizes are prepared. In spite of its enormous impact, however, there are critical shortcomings that limit the scope of this important class of transformations;[1] a full range of catalyst-controlled *Z*- or *E*-selective processes for formation of di- or trisubstituted alkenes are among crucial but difficult challenges that remain unaddressed. Solutions to such shortcomings require the design of efficient and stereoselective catalysts, a task that demands a more complete appreciation of the fundamental mechanistic principles that govern OM.

A unique characteristic of OM, illustrated in Scheme 1A, is that the M=C bond undergoes a "side change" on each occasion a metallacyclobutane (mcb) is formed and cleaved to reveal a different carbene complex.[2] A ring-closing metathesis (RCM) or cross-metathesis (CM) reaction thus proceeds via several mcb intermediates and involves a string of side changes. With a stereogenic-at-metal complex containing a chiral ligand, a "side change" implies a stereochemical inversion and formation of energetically distinct and spectroscopically detectable diastereoisomeric entities characterized by individual reactivity and selectivity profiles. A better appreciation of the relative reactivity of each isomeric complex is central to our understanding of the mechanistic nuances of OM, since such factors influence reactivity and/or stereoselectivity of a transformation.

Diastereomeric carbene complexes may interconvert by non-OM-based pathways as well as through processes that are generally referred to as polytopal rearrangements (Scheme 1B).[3] Such stereoisomeric interconversions are relevant to catalytic OM, since high reactivity and/or stereoselectivity depends on each diastereomeric complex participating in a separate segment

Scheme 1. Two Distinct Rearrangement Pathways Available to Pentacoordinate Ru-Based Carbene Complexes

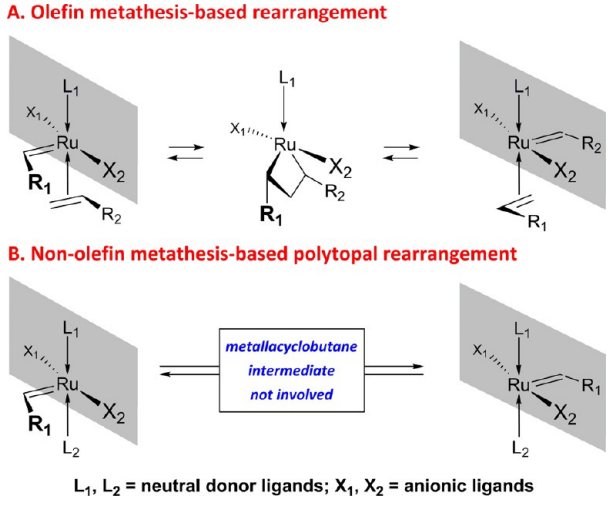

Received: October 16, 2013
Published: February 17, 2014

   dx.doi.org/10.1021/ja410606b | J. Am. Chem. Soc. 2014, 136, 3439−3455

Scheme 2. Different Types of Ru-Based Complexes Used in Catalytic Olefin Metathesis

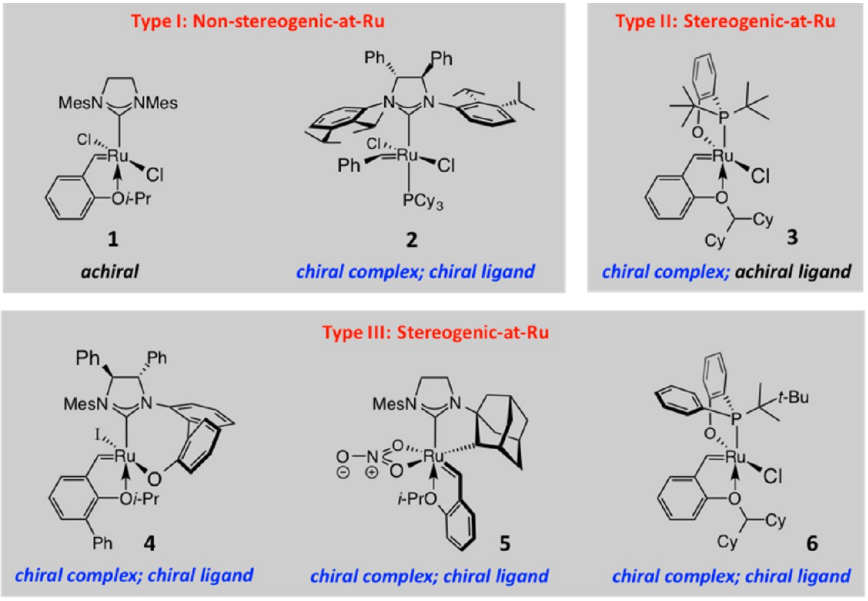

of the catalytic cycle, and non-OM-based isomerizations can cause diminished yields and low diastereo- or enantiomeric ratios (dr and er, respectively). Additionally, catalytic OM is a type of polytopal rearrangement, meaning that a detailed comprehension of the principles that govern non-OM-based isomerizations might lead to a more perceptive analysis of selectivity and reactivity trends, as well as impart information needed for the design of more effective and stereoselective catalysts.

Herein, we first present the results of our studies regarding thermally induced and Brønsted acid catalyzed polytopal isomerization of stereogenic-at-Ru carbene complexes. By means of extensive DFT calculations, key electronic factors that influence the facility of the aforementioned rearrangements—particularly those originating from the anionic ligands—are elucidated; this includes analysis of the impact of a proton Lewis acid on the rate of various polytopal rearrangements. In the concluding segment, the relationship between the principles that govern non-OM-based isomerizations and those that have an effect on catalytic OM reactions are scrutinized in three different settings: (1) We analyze the role of the electronic effects that originate from the anionic ligands of a Ru complex on the rate of a representative OM process. (2) We probe the electronic factors involving anionic ligands that give rise to the more facile OM transformations with allylic alcohols. (3) We dissect the electronic principles that have culminated in the successful design of Ru-based complexes for *Z*-selective OM.

RESULTS

1. Polytopal Rearrangements and Relevance to Catalytic Olefin Metathesis. Interconversion of metal carbenes via mcb complexes entails reorganization of the ligands surrounding the transition metal in a manner akin to a polytopal rearrangement.[4−6] OM-based isomerizations engender diverse outcomes, depending the metal complex involved. A Ru carbene can belong to three general stereochemical categories (Scheme 2): Type I pertains to nonstereogenic-at-Ru complexes that are either achiral (e.g., **1**)[7] or contain a chiral ligand (e.g., **2**).[8] Furthermore, there are stereogenic-at-Ru carbenes that may be divided into two different sets: Type II, comprised of complexes with only achiral ligands (e.g., **3**),[2c−e] and Type III, which contain a chiral ligand (e.g., **4**-**6**).[2c−g,9−11]

In the case of a Type I system (Scheme 3A), a square pyramidal (sp) olefin π complex (**7**) undergoes degenerate OM via a trigonal bipyramidal (tbp) mcb (**8**).[12] Due to the enantiotopic (e.g., **1**) or diastereotopic (e.g., **2**) relationship of the anionic ligands (Cl), such a side change or "stereochemical inversion" is not detectable. On the contrary, with stereogenic-at-

Scheme 3. Olefin Metathesis-Based Polytopal Rearrangements with Different Types of Ru-Based Complexes

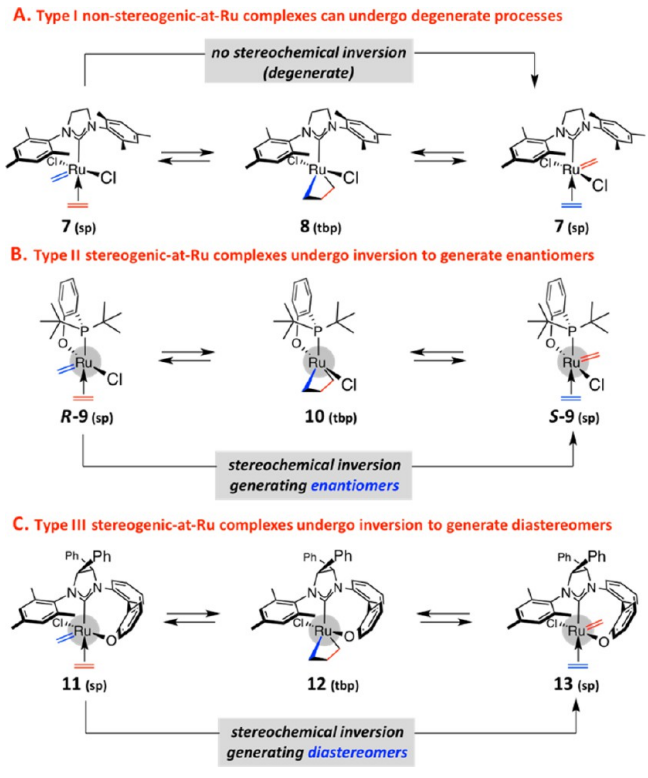

dx.doi.org/10.1021/ja410606b | J. Am. Chem. Soc. 2014, 136, 3439−3455

Scheme 4. Non-Olefin Metathesis-Based Polytopal Rearrangement Pathways with Stereogenic-at-Ru (Type III) Complexes

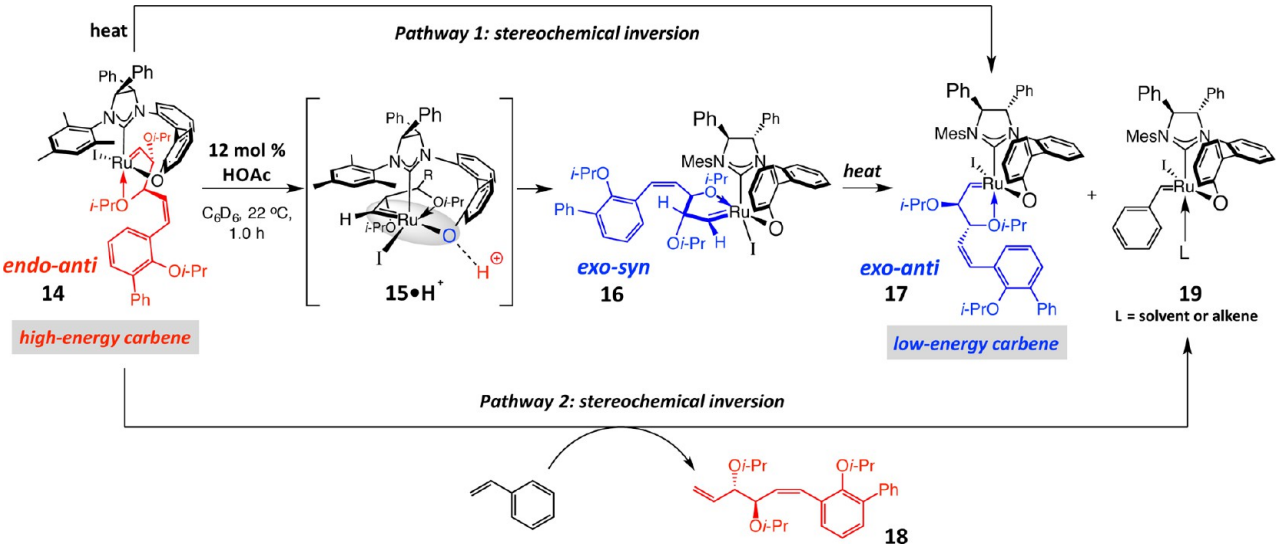

Ru carbenes, nonproductive OM results either in the interconversion between two enantiomeric (Scheme 3B; *S*-**9** → *R*-**9** via **10**) or diastereomeric forms (Scheme 3C; **11** → **13** via **12**). In the latter instance (**11** → **13**), the difference in reactivity between the chemically distinct Ru−olefin complexes can allow an OM transformation to proceed with exceptional chemoselectivity.[2c−g] Such attributes have been exploited toward the design of alternating copolymerization[2c−g] and ring-opening/cross-metathesis (ROCM).[9,13] It should be mentioned that chemoselectivity has been observed in OM reactions promoted by nonstereogenic-at-Ru complexes that contain unsymmetrically substituted monodentate NHC ligands; in these instances, generation of diastereomeric carbene species hinges on the barrier for rotation around the Ru−C^{NHC} bond.[14]

To obtain additional information regarding the pathways that are available for facile interconversion of the diastereoisomeric complexes, we isolated and characterized a high-energy Ru carbene diastereomer **14*endo-anti*** (Scheme 4), and investigated its fluxional behavior.[3,15−17] (The term ***endo*** refers to a carbene that is pointing within the cavity generated by the biphenyl bridge; the term ***exo*** is indicative of a Ru=C that is positioned below the mesityl substituent of the NHC moiety. Similarly, ***syn*** and ***anti*** denote complexes wherein the carbene unit's isopropoxy group is chelated to the Ru center cis or trans to the NHC ligand, respectively.) We determined that, without an alkene present, thermally induced stereochemical inversion by non-OM-based polytopal rearrangement leads to the formation of the thermodynamically favored diastereomer **17*exo-anti***. We demonstrated that non-OM-based rearrangement of **14*endo-anti*** to **17*exo-anti*** (Scheme 4), conversion of **14*endo-anti*** to **17*exo-anti*** (pathway 1), and CM of **14*endo-anti*** with styrene to generate **18** and *exo* benzylidene **19** (pathway 2) are competitive. We showed that the latter events occur on a similar time scale and are therefore capable of perturbing OM reaction sequences and can culminate in low efficiency and stereoselectivity.[3] Nevertheless, the chemoselectivities observed in the alternating copolymerization with complex **6** (Scheme 2) suggest that the distinct diastereomeric carbene species (Scheme 3C) can maintain a certain degree of configurational stability,[2h] and that non-OM-based polytopal rearrangements might require higher energy barriers.

We subsequently discovered that the addition of a Brønsted acid (e.g., 12 mol % HOAc) facilitates the conversion of **14*endo-anti*** to **16*exo-syn***, which is an intermediate en route to **17*exo-anti***.[3] We proposed that the latter rearrangement could involve transition state **15•H**$^+$ (Scheme 4), such that donor−donor electronic repulsion arising from the trans relationship between the carbene and the anionic phenoxide ligand is minimized. We posited that the above observations are relevant to the mechanism of OM reactions, as the same energy-raising donor−donor interactions could diminish mcb stability to reduce reaction rates, particularly in cases where cycloaddition is turnover-limiting.

2. Computational Studies.[18] *2.1. General Considerations.* To carry out the computational investigations, we opted for the structurally truncated complexes shown in Scheme 5. The omission of the diphenyl backbone, the *p*-methyl group of the mesityl substituent, the side chains of the bidentate alkylidene, as well as the exchange of the isopropyl for a methyl group on the chelating ether oxygen (O^2), was to achieve minimal conformational complexity and for reducing computational cost. The reaction coordinate involving the complexes in Scheme 5, wherein the two carbene ligands [i.e., the NHC (C^1) and the alkylidene (C^2)] and the Ru center are held at a fixed position, were investigated.

Scheme 5. Structurally Truncated Complexes Used in the Computational Studies

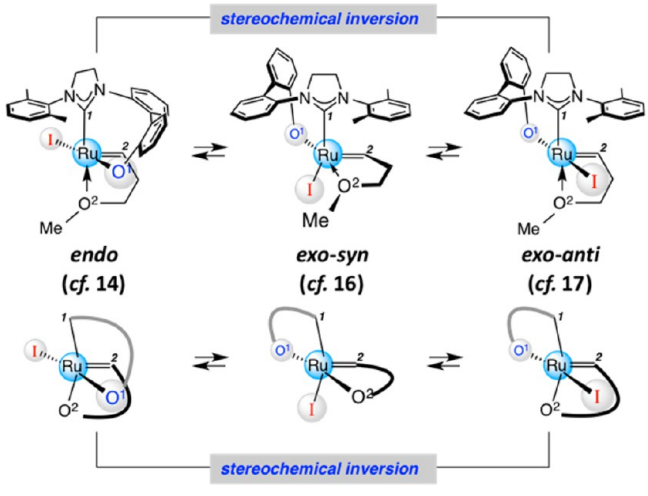

dx.doi.org/10.1021/ja410606b | J. Am. Chem. Soc. 2014, 136, 3439−3455

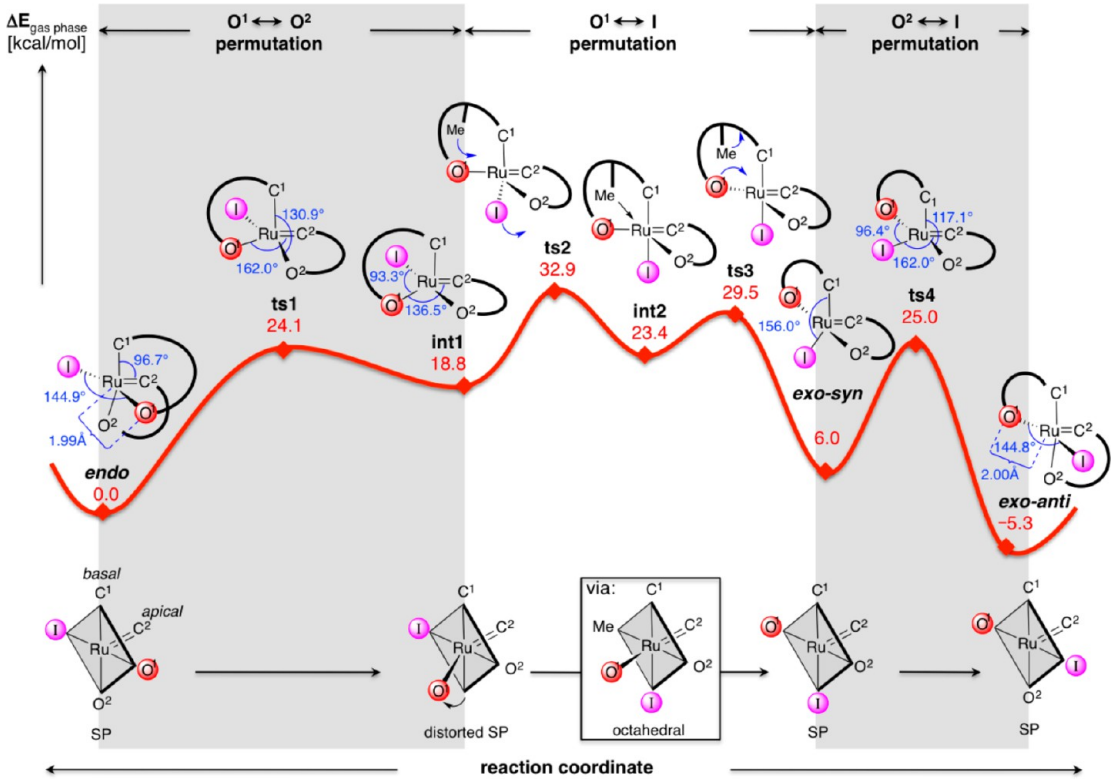

Figure 1. Computed potential energy surface in gas phase (PES; BP86/basis1) illustrating the thermally induced polytopal rearrangement that results in stereochemical inversion of the Ru carbene complex (***endo*** → ***exo-anti***). For a complete list of bond lengths and angles, a three-dimensional representation of the PES, and an illustrative animation, see the Supporting Information; sp = square pyramidal, ts = transition state, int = intermediate.

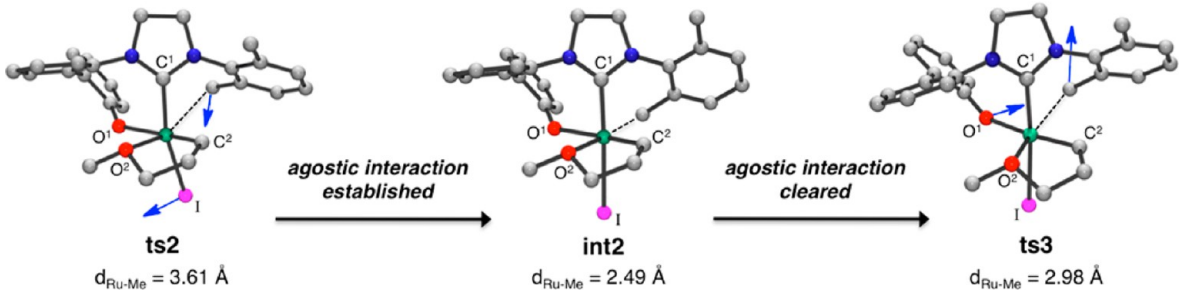

Figure 2. Computed structures (BP86/basis1) for formation of octahedral intermediate **int2** (via **ts2**) and its rearrangement through **ts3**; H atoms are omitted for clarity; d_{Ru-Me} = distance between the Ru and C atoms of the *o*-methyl group.

From the suggested perspective, stereochemical inversion (***endo*** → ***exo-anti***) results in the rotation of the NHC group and concomitant transposition of the anionic phenoxide (O^1) and iodide (I) ligands.

2.2. Thermally Induced Polytopal Rearrangements. The calculated potential energy surface in Figure 1 corresponds to the thermal polytopal rearrangement of the higher energy, but kinetically stable, ***endo*** carbene (sp geometry, apical alkylidene carbene C^2;[19] see lower portion of Figure 1) to the corresponding thermodynamically preferred ***exo-anti*** diastereomer (E_{rel} = −5.3 kcal/mol). The initial conversion of ***endo*** to the isolable sp ***exo-syn*** (E_{rel} = 6.0 kcal/mol) involves a series of isomerizations that proceed via two additional structures that have not been observed spectroscopically: **int1**, possessing a distorted sp geometry with the basal anionic O^1 ligand deviated out of plane, and octahedral **int2** arising from a C−H/Ru agostic interaction. The barrier associated with **ts2** (32.9 kcal/mol) is rate limiting, and the final ***exo-syn*** to ***exo-anti*** transformation takes place via a single transition state (**ts4**, E_{rel} = 25.0 kcal/mol). The overall process thus consists of three permutations, each leading to an exchange between two basal ligands (see bottom of Figure 1). The result of the first sequence (***endo*** → **ts1** → **int1**) is the interchange of O^1 and O^2, whereas the final succession (***exo-syn*** → **ts4** → ***exo-anti***) entails the swapping of I for O^2. The net result of transformation of **int1** to ***exo-syn*** is the transposition of the anionic ligands (O^1 and I). The latter interconversion proceeds stepwise via **ts2**, **int2**, and **ts3** and involves a change in coordination number (five → six → five) because of the formation and rupture of a C−H/Ru agostic interaction involving an NHC methyl group.

The progression in Figure 1 commences with the widening of the O^1−Ru−C^2 angle from ***endo*** to **ts1**, which results in the tightening of the O^2−Ru−C^1. Next, recontraction of the O^1−Ru−C^2 angle generates **int1**, the distorted sp geometry of which is likely imposed by the bidentate NHC, preventing relaxation to an sp arrangement. Next, the permutation of O^1 and I proceeds via octahedral **int2**, which is the highest energy intermediate, probably since anionic groups O^1 and I are trans to electron donor units C^2 and C^1, respectively. The expansion of the O^1−Ru−C^2 in **ts2** causes the iodide to reside trans to C^1; this is facilitated by a C−H/Ru agostic interaction involving a mesityl *o*-methyl group (Figure 2). The distance between the Ru atom and the *o*-methyl in **ts2** decreases from 3.61 Å to 2.49 Å when **int2** is formed. The sterically congested octahedral **int2**, which contains a tridentate, a bidentate, as well as a monodentate ligand, undergoes a dissociative

dx.doi.org/10.1021/ja410606b | J. Am. Chem. Soc. 2014, 136, 3439−3455

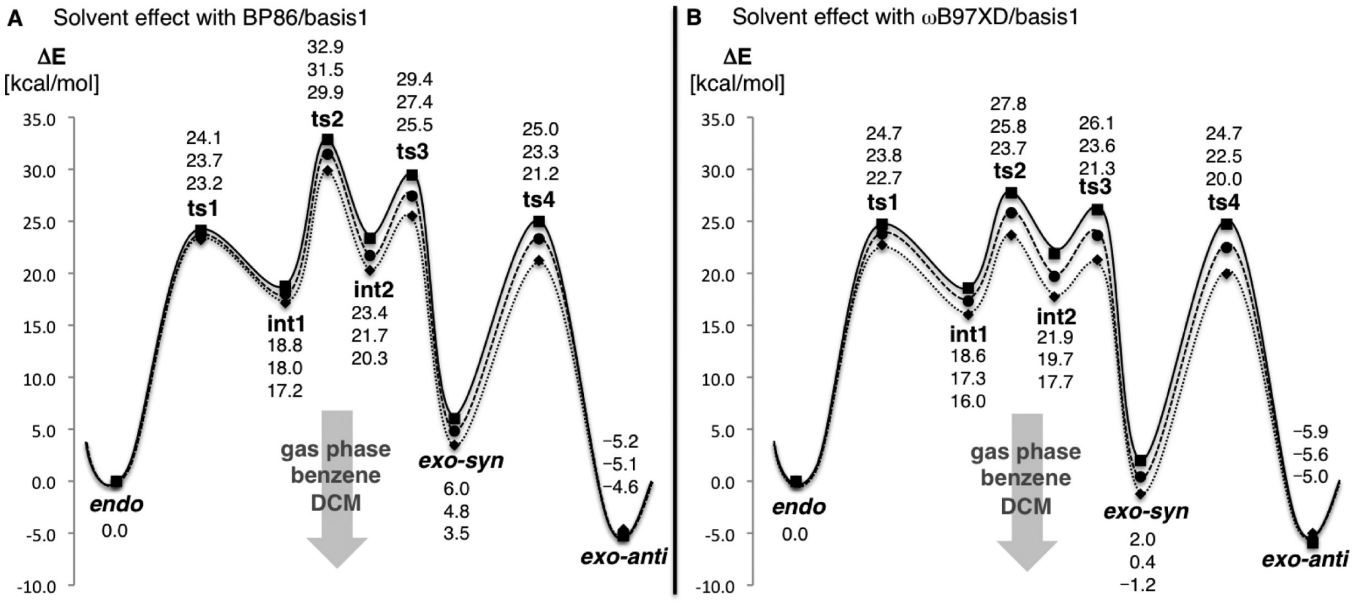

Figure 3. Evaluation of solvent effects for the thermally induced rearrangement of ***endo*** to ***exo-anti*** with density functionals BP86 and ωB97XD. For analysis of solvent effects with the M06 functional, see the Supporting Information.

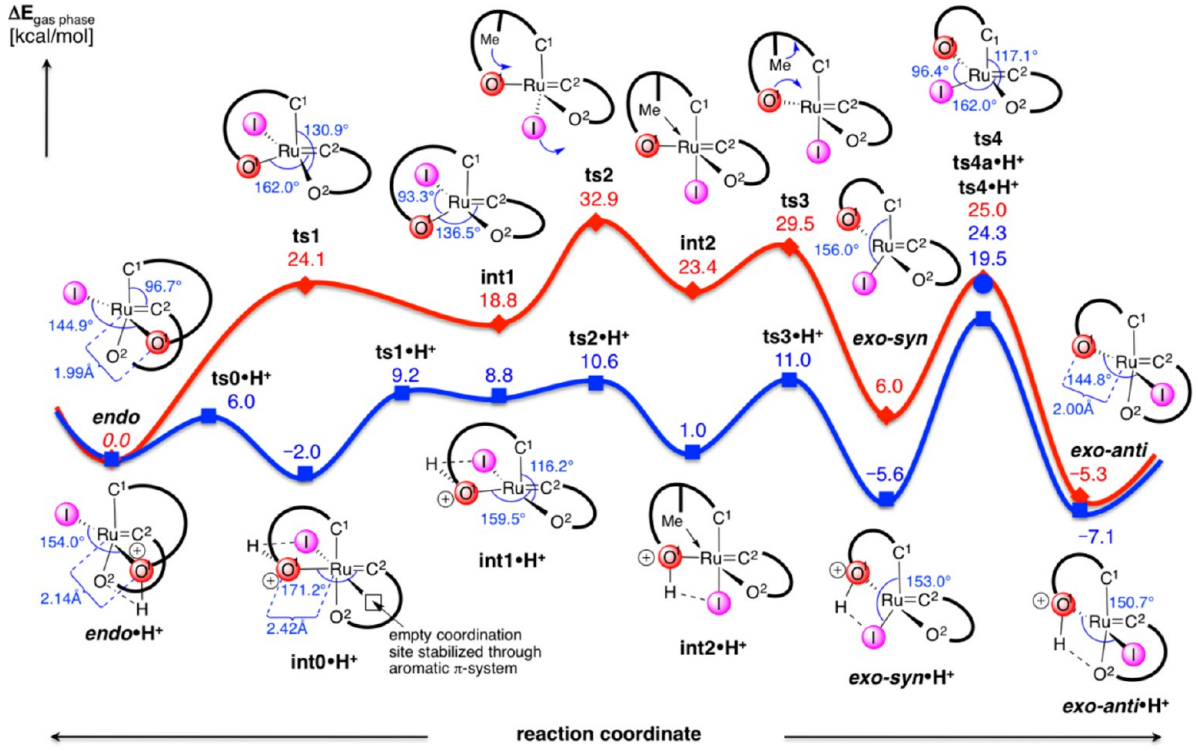

Figure 4. Comparison of the computed potential energy surfaces in gas phase (PESs; BP86/basis 1) for the thermally induced (**red**) and proton-catalyzed (**blue**) polytopal rearrangements (***endo*** → ***exo-anti*** and ***endo***•H^+ → ***exo-anti***•H^+, respectively). For bond lengths and angles, see the Supporting Information; ts = transition state, int = intermediate.

ligand displacement en route to ***exo-syn***. The C−H agostic interaction is removed upon movement of O^1, a structural adjustment manifested by the increase in distance between the transition metal center and the carbon atom of the *o*-methyl group to 2.98 Å in **ts3** (cf. Figure 2) when the O^1−Ru−C^2 angle contracts. The structure of ***exo-syn*** resembles an sp geometry[19] wherein the iodide is distorted out-of-plane (I−Ru−C_1 = 156.0°). The final step is the rearrangement of O^1 and I from a cis orientation in ***exo-syn*** to the thermodynamically preferred trans alignment in ***exo-anti***; the widening of the I−Ru−C^2 angle in **ts4** makes available a coordination site trans to C^1 that can be occupied by O^2. Complex ***exo-anti*** is thus generated by the I−Ru−C^2 angle becoming smaller.

It should be noted that we have compared the results shown in Figure 1 (BP86) with the performance of recently developed density functionals that have been corrected for the treatment of dispersion interactions. Application of M06 and ωB97XD functionals does not appear to have a significant effect on the qualitative description of the potential energy surface presented in Figure 1 (Figure 3, solid curves). Quantitatively, however, a minor to significant reduction of the overall barrier (**ts2**) is predicted (32.9, 31.0, and 27.8 kcal/mol for BP86, M06,

dx.doi.org/10.1021/ja410606b | J. Am. Chem. Soc. 2014, 136, 3439−3455

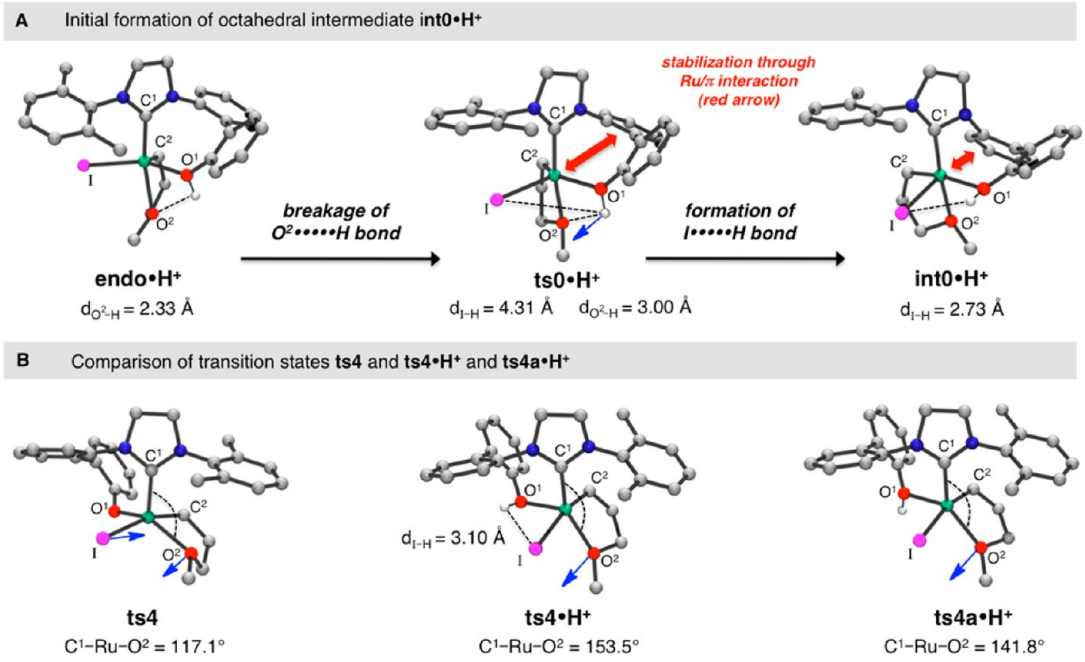

Figure 5. Selected computed structures (BP86/basis1) for the proton-catalyzed polytopal rearrangement including displacement vectors in transition states; H atoms are omitted for clarity; int = intermediate, ts = transition state.

and ωB97XD, respectively) and a similar stabilization is calculated for the intermediate ***exo-syn*** (6.0, 3.4, and 2.0 kcal/mol for BP86, M06, and ωB97XD, respectively).

Next, we turned to probing the influence of different organic solvents of varying polarities on single-point energy calculations (Figure 3, dashed curves). Through application of the BP86 functional we established that benzene lowers the energy of **ts2** by 1.4 kcal/mol and dichloromethane has a stronger influence in the same direction (3.0 kcal/mol, Figure 3A); similar stabilizations were observed for **int2** → **ts4**. Calculations in dichloromethane (ωB97XD) point to an overall barrier as low as 23.7 kcal/mol (**ts2**) and a reduction in the energy of ***exo-syn*** to the extent that, in line with the experimental findings, it becomes more stable than ***endo*** (−1.2 kcal/mol, Figure 3B). On the other hand, changing the density functional or polarity of the medium has minimal effect on the relative energy of ***endo*** and ***exo-anti*** (see below for further discussion regarding dipolar effects). The inclusion of the diphenyl backbone in modeling studies resulted in a small increase in the energies of **ts1**, **int1**, and **ts4** (by 2.3, 3.9, and 2.4 kcal/mol, respectively), exerting negligible influence on the relative energy between ***endo*** and ***exo-anti***.[20]

2.3. Acid-Catalyzed Polytopal Rearrangement. We have investigated the potential energy surface for the transformation of the ***endo*** complex in the gas phase, wherein the anionic phenoxide (O^1) is protonated (***endo*•H$^+$**, blue curve, Figure 4). Although the ligand movement occurs in a similar manner compared to the thermally induced variant (red vs blue curve), distinct structural attributes are evident. Importantly, there is a significant lowering of the barrier for the conversion of ***endo*•H$^+$** to ***exo-syn*•H$^+$** (E_{rel} for **ts2•H$^+$** = 10.6 kcal/mol vs 32.9 kcal/mol for **ts2**). What is more, a new intermediate **int0•H$^+$** is located in addition to **int1•H$^+$** and **int2•H$^+$**, and there is a change in the highest energy point from **ts2** in the thermally induced polytopal rearrangement to **ts4•H$^+$** in the proton-catalyzed process (E_{rel} = 19.5 kcal/mol).

Examination of the Brønsted acid promoted reaction coordinate (Figure 4, left to right) provides other noteworthy information regarding the effect of the Lewis acid. One consequence of phenoxide (O^1) protonation is the elongation of the Ru−O^1 bond from 1.99 Å in ***endo*** to 2.14 Å in ***endo*•H$^+$**. Moreover, an additional H-bond involving the O^2 ligand is generated due to the propinquity of the two oxygen ligands (O^1 and O^2). Thus, as illustrated in Figure 5A, there is an initial expansion of O^1−Ru−C^2 angle in ***endo*•H$^+$** that generates the octahedral **int0•H$^+$** in order to allow for the formation of an H-bond with the iodide ligand. Consequently, the O^2···H distance increases from 2.33 Å in ***endo*•H$^+$** to 3.00 Å in **ts0•H$^+$**, while the I···H is reduced from 4.31 Å in **ts0•H$^+$** to 2.73 Å in **int0•H$^+$**. Another notable attribute of this pathway is that the available coordination site trans to the iodide in **int0•H$^+$** appears to be stabilized by the π-electron density of the aromatic unit of the biphenyl bridge (Figure 5A). Ensuing movement of O^2 trans to the halide generates sp complex **int1•H$^+$**. In comparison with the thermally promoted process, in which the **int1** → **int2** rearrangement is associated with a barrier of 14.1 kcal/mol, conversion of **int1•H$^+$** to the octahedral complex **int2•H$^+$** requires no more than 1.8 kcal/mol.

Complex **ts4•H$^+$** (E_{rel} = 19.5 kcal/mol) holds a proton bridge that links anionic ligands O^1 and I (distance for I···H = 3.10 Å, Figure 5B), leading to its stabilization relative to the neutral form (**ts4**, E_{rel} = 25.0 kcal/mol). Additionally, we were able to locate transition state structure **ts4a•H$^+$** (blue circle in Figure 4; E_{rel} = 24.3 kcal/mol), which is energetically similar to **ts4** likely because the proton is not associated with the iodide (Figure 5B, right side). The stabilization offered by **ts4•H$^+$** appears to be insufficient to allow for conversion of the ***exo-syn*** to the ***exo-anti*** complex to be accelerated in the presence of acetic acid.

DISCUSSION

1. The Driving Force for Rearrangement of *endo* to *exo-anti* Carbene. The computational studies detailed above involve processes that have a higher energy ***endo*** carbene as their starting point. Why is an endo complex energetically less favored?

The origin of the energy difference between ***endo*** and ***exo-anti*** complexes can be found in the structural analysis depicted in Figure 6. In the ***endo*** complex the mesityl substituent is rotated to situate it above the iodide ligand as a result of the smaller I−Ru−C^1−N dihedral angle (40.2° in ***endo*** vs 92.2° in ***exo-anti***, Figure 6, parts A and A′). Such geometry produces steric strain between the iodide and the mesityl ring, as indicated by the reduced C^{ortho}−I and C^{Me}−I distances in the ***endo*** isomer (3.70 and 4.04 Å vs 4.78 and 4.12 Å in ***exo-anti***); as a consequence, the mesityl substituent is forced to tilt (C^1−N−C^{ipso}−C^{ortho} dihedral angle of 113.0° vs 100.6° in ***exo-anti***, Figure 6, parts B and B′).

dx.doi.org/10.1021/ja410606b | J. Am. Chem. Soc. 2014, 136, 3439−3455

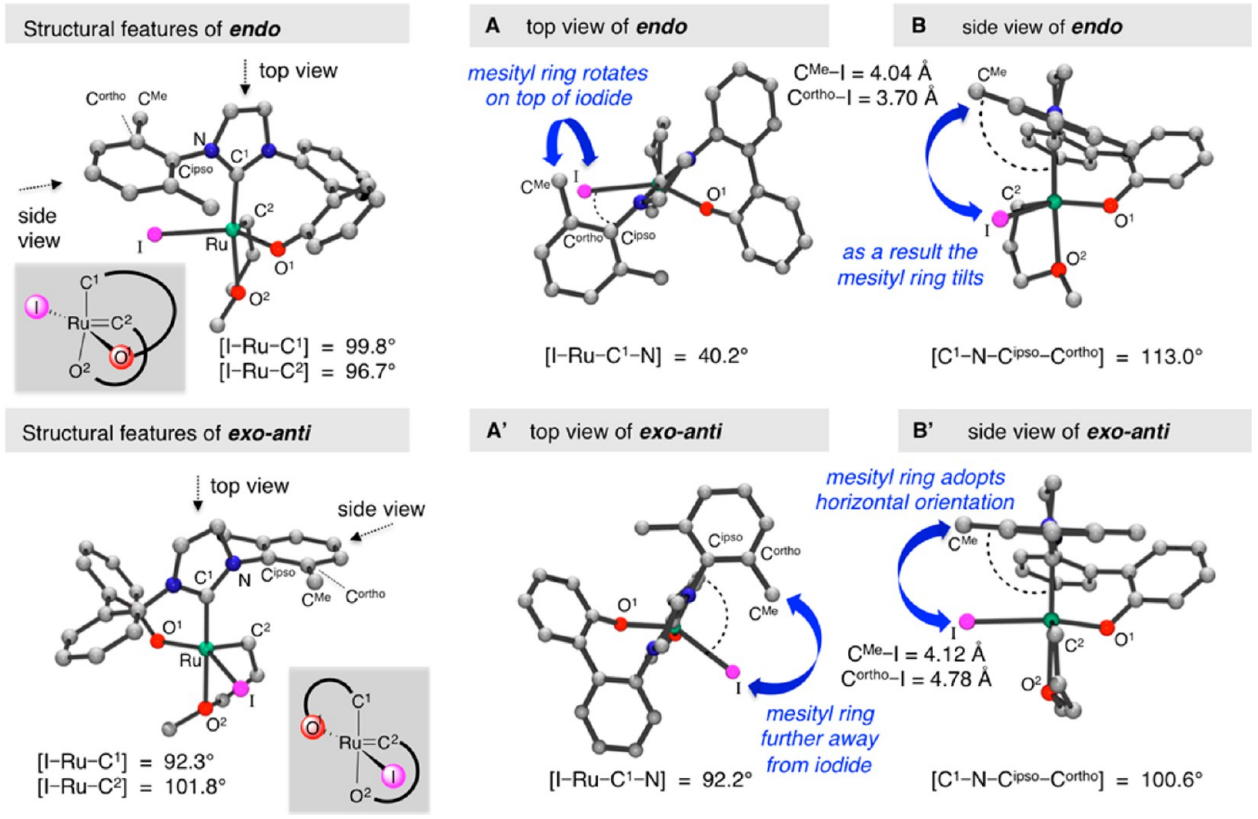

Figure 6. Analysis and comparison of representative key structural features of ***endo*** and ***exo-anti*** (BP86/basis1).

The wider I–Ru–C_1 (99.8° in ***endo*** vs 92.3° in ***exo-anti***) and the contracted I–Ru–C^2 angles (96.7° in ***endo*** vs 101.8° in ***exo-anti***) are consistent with there being a more severe repulsion between the iodide and mesityl substituents within the ***endo*** complex. We did not detect a significant influence by the diphenyl backbone and polar media on the relative energy between ***endo*** and ***exo-anti*** (see above).

2. Interactions Contributing to Rearrangement Rates and the Influence of a Brønsted Acid Catalyst. In spite of the stereochemical inversion being exothermic by 5.3 kcal/mol, the higher energy ***endo*** complex can be isolated by routine silica gel chromatography.[3] The basis of the contrast between energetics and kinetic stability is 2-fold: donor–donor interactions and dipolar effects arising from the anionic ligands. Below, we dissect the origin of the kinetic stability of the ***endo*** complex and provide a rationale for why the aforementioned factors are minimized by a Brønsted acid, leading to the isolation of the lower energy ***exo-syn*** isomer but not the energetically most favored ***exo-anti*** complex.

2.1. Donor–Donor Interactions Involving Anionic Ligands. The destabilizing interactions between the O^1 and I and neutral electron donating carbene C^1 and C^2, which arise from their residing opposite to one another (trans influence), may be qualitatively evaluated by calculating the negative charge accumulation on the anionic ligands as a function of the reaction coordinate (Figure 7).[21] Three distinct donor–donor interactions (A, B, and C) emerge through examination of the structures of intermediates and transition states associated with the thermally induced rearrangement (Figure 7, top): (A) O^1 trans to C^2 in **ts1**, **ts2**, **int2**, and **ts3**; (B) iodide trans to C^1 in **ts2**, **int2**, **ts3**, and ***exo-syn***; and (C) iodide trans to C^2 in **ts4**.

2.1.1. Interactions Involving the Anionic O^1 Ligand (labeled A, top of Figure 7). The graphical representation of the O^1–Ru–C^2 angle as a function of the reaction coordinate indicates two maxima at 162.0° and 170.6°, the first of which corresponds to **ts1** and the second includes **ts2**, **int2**, and **ts3**, peaking at **int2** (Figure 7a, red curve). A strong trans influence is manifested by elongation of the Ru–O^1 bond (1.99 Å in ***endo*** to 2.07 Å in **ts1** and 2.17 Å in **ts2**; Figure 7b, red curve). The concomitant negative charge accumulation (APT charges) on the phenoxide O^1, illustrated in Figure 7c, is consistent with an analogous repulsive interaction between the same anionic ligand and the C^2 of the Ru=C unit. The diminution of destabilizing donor–donor interactions involving anionic O^1 as a result of its protonation becomes markedly evident when the rearrangement of **int1** → **int2** is compared to **int1**•H^+ → **int2**•H^+. The distorted sp geometry of **int1** probably originates from minimization of a strong trans influence caused by the O^1 and C^2 ligands, as represented by the relatively deep local minimum shown in Figure 7a (red curve). The higher barrier for **ts2** (E_{rel} = 32.9 kcal/mol), which is responsible for the unusual kinetic stability of ***endo***, is likely because subsequent rearrangement to generate **int2** necessitates an expansion of the O^1–Ru–C^2 angle and the overcoming of unfavorable donor–donor interactions. In contrast, the elongation of the Ru–O^1 bond in **ts2**•H^+ (2.54 Å vs 2.17 Å in **ts2**) resulting from protonation of O^1 translates to a lesser amount of donor–donor repulsion in **int1**•H^+, leading to its sp geometry (cf. shallow minimum in Figure 7a, blue curve) to render **ts2**•H^+ more energetically accessible (E_{rel} = 10.6 kcal/mol).

2.1.2. Interactions Involving the Anionic Iodide Ligand (labeled B and C, top of Figure 7). The plots of the I–Ru–C^1 and I–Ru–C^2 angles as a function of the reaction coordinate

dx.doi.org/10.1021/ja410606b | J. Am. Chem. Soc. 2014, 136, 3439–3455

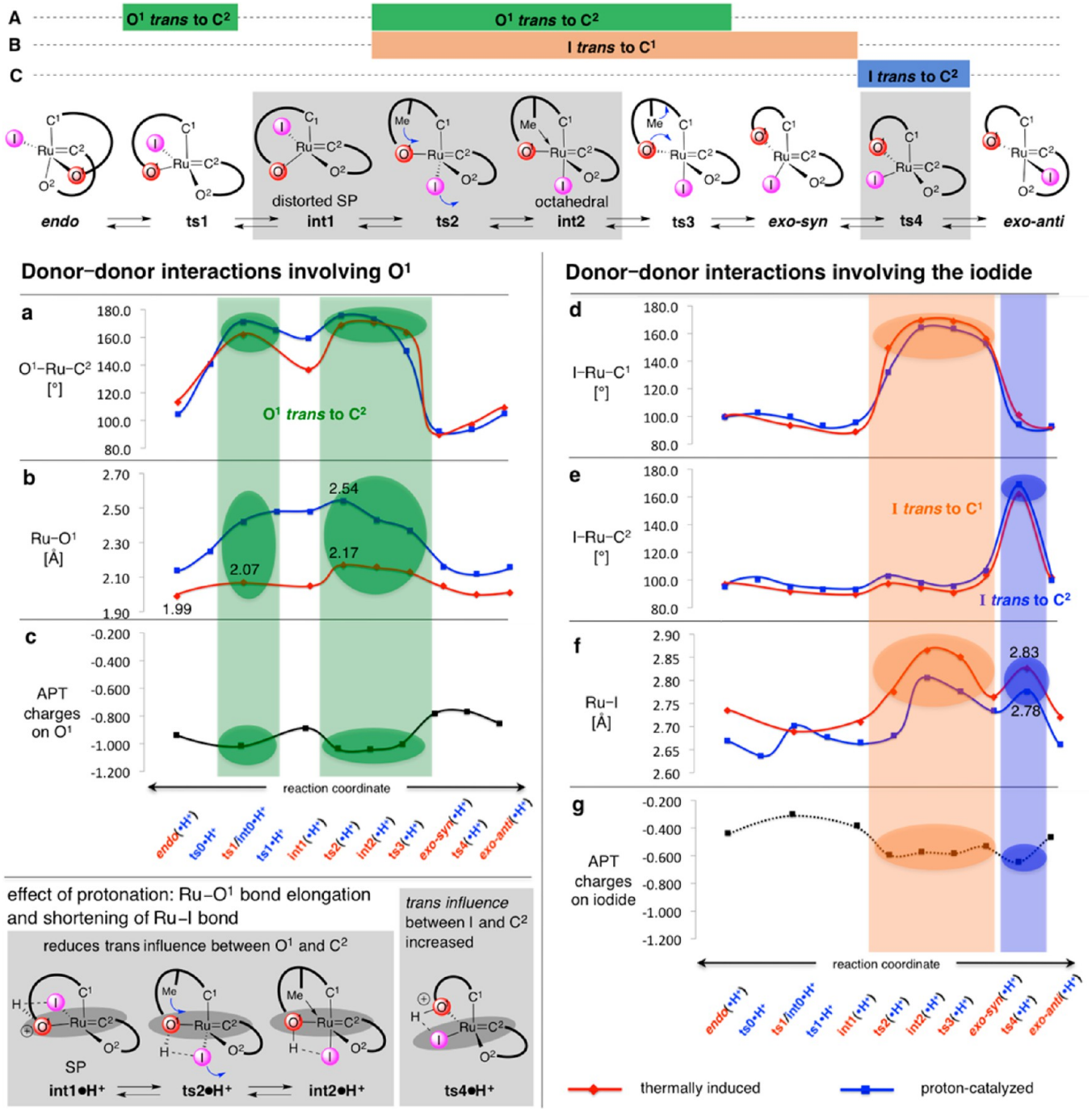

Figure 7. Analysis of donor–donor interactions (BP86/basis1, in gas phase) that contribute to the barrier for polytopal rearrangement from ***endo*** to ***exo-syn*** complex and their minimization as a result of protonation; ts = transition state, int = intermediate.

reveal that the iodide ligand is situated trans to C^1 in **ts2**, **int2**, **ts3**, and ***exo-syn*** (Figure 7d), whereas it resides opposite to C^2 in **ts4** (Figure 7e). Additionally, the two maxima in parts d and e of Figure 7 correlate with the longer Ru–I bond lengths (Figure 7f, red curve), leading to electron density accumulation on the halide; the most negative partial charge on the iodide is in **ts4** (Figure 7g). One consequence of O^1 protonation is the shortening of the Ru–I bond (2.83 Å in **ts4** to 2.78 Å in **ts4•H⁺**, cf. Figure 7f, blue curve), which is likely due to enhanced Lewis acidity of the transition metal in the protonated complex. Unlike the positive effect of a proton on the minimization of donor–donor interactions between O^1 and C^2 in **ts2•H⁺**, the trans influence between the I and C^2 ligands is not minimized in **ts4•H⁺**, probably because the halide alone represents a relatively inferior H-bond acceptor. Consequently, **ts4•H⁺** emerges as the rate-limiting transition state under acid-catalyzed conditions. These findings explain why the acid-catalyzed process does not proceed beyond the formation of ***exo-syn*** (cf. blue curve, Figure 4), whereas the thermal protocol delivers the lowest energy ***exo-anti*** complex.

2.2. Dipolar Interactions. A sizable dipole moment is the consequence of charge separation within a molecule, leading to its relative destabilization in the gas phase compared to a polar medium.[17] In a polytopal rearrangement, there is charge

dx.doi.org/10.1021/ja410606b | J. Am. Chem. Soc. 2014, 136, 3439–3455

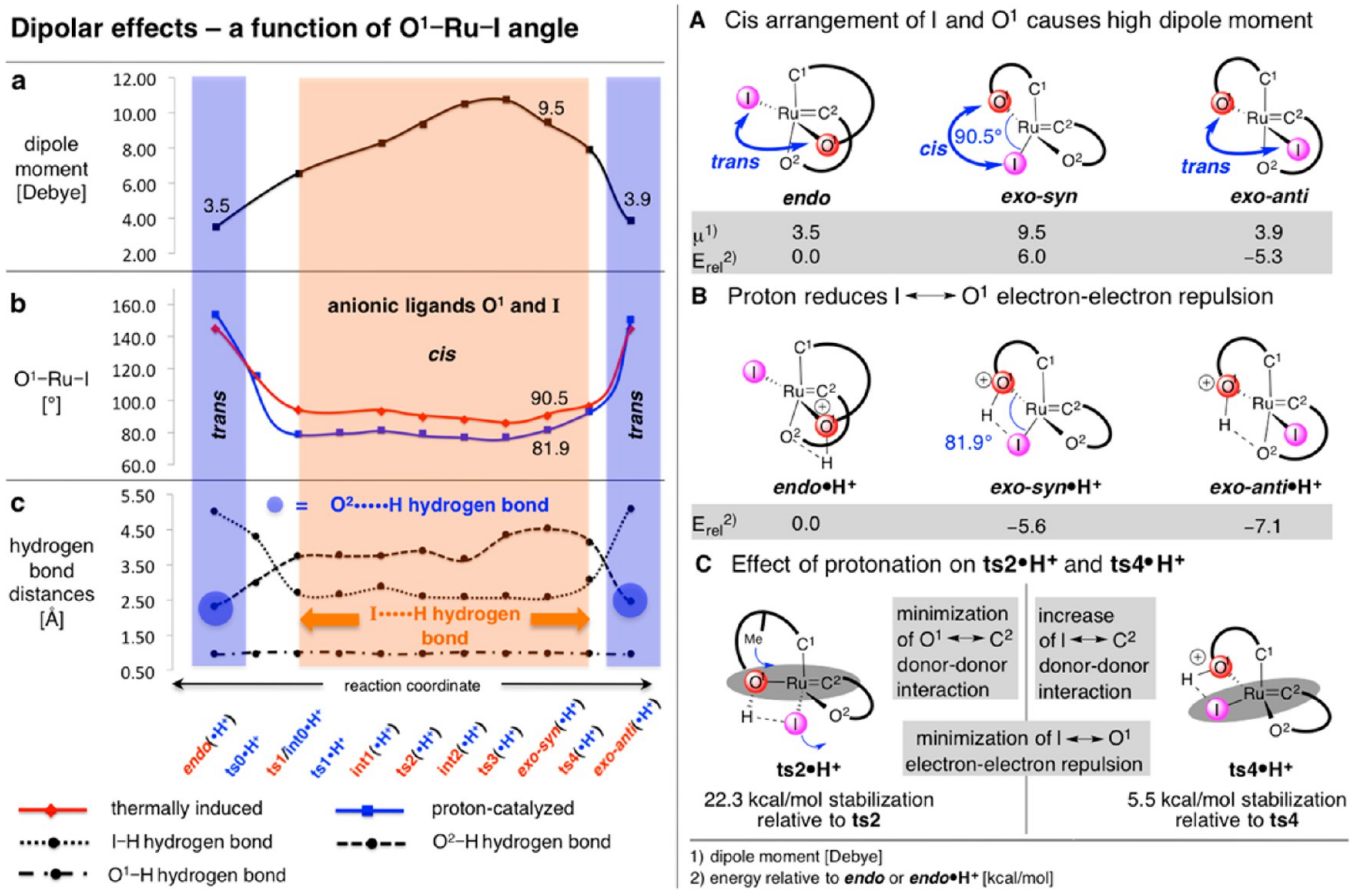

Figure 8. Analysis of dipolar effects (BP86/basis1, in gas phase) that contribute to the barrier for polytopal rearrangement from ***endo*** to ***exo-syn*** complex and the influence of a bound proton; ts = transition state, int = intermediate.

redistribution among the ligands, altering dipole moments, leading to attendant increase or decrease in repulsive forces especially between anionic ligands. Analysis of the ***endo*** to ***exo-anti*** isomerization points to a substantial degree of dipolar effects (cf. Figure 8).

Representation of dipole moments as a function of the reaction coordinate, depicted in Figure 8a, suggests a strong correlation with the O¹–Ru–I angle (Figure 8b, red curve). The increased polarity of ***exo-syn*** (9.5 D, Figure 8A) originates from the syn arrangement of the anionic ligands (O¹ and I), whereas their anti relationship points to an overall dipole minimization, as observed in ***endo*** and ***exo-anti*** complexes (3.5 and 3.9 D, respectively). The high dipole moment of ***exo-syn*** (vs ***endo***) is likely the reason for its destabilization in the gas phase (E_{rel} = 6.0 kcal/mol), while there is a significant lowering of its energy in polar media (see above).

A consequence of the O¹ protonation is the lowering of electron–electron repulsion between the lone pairs on the anionic ligands that are in a syn relationship; this is evidenced by the decrease in O¹–Ru–I angle (90.5° in ***exo-syn*** vs 81.9° in ***exo-syn*•H⁺**; Figure 8b, blue curve). We calculate that ***exo-syn*•H⁺** is stabilized by 11.6 kcal/mol relative to ***exo-syn***, whereas ***exo-anti*•H⁺** is only 1.8 kcal/mol lower in energy compared to ***exo-anti*** (Figure 8A,B). The generation of secondary H-bonds, as shown in Figure 8c, underscores the ability of a proton to decrease electronic repulsion through more than a single point of contact. The O²···H interaction in ***endo*•H⁺**, which gives rise to diminution of charge repulsion between the anionic O¹ and the neutral O², is ruptured in favor of an H-bond with the iodide in **int0•H⁺** → **ts4•H⁺**. The O²···H association is re-established in ***exo-anti*•H⁺** when the I···H interaction is no longer viable.

The impact of dipolar effects on transition states **ts2•H⁺** and **ts4•H⁺** is illustrated in Figure 8C. In addition to reducing donor–donor interactions between O¹ and C² in **ts2•H⁺**, minimization of electron–electron repulsion between the lone pairs on the anionic ligands leads to substantial stabilization relative to **ts2** (−22.3 kcal/mol). On the other hand, the higher donor–donor interaction between I and C² in **ts4•H⁺** (cf. Figure 7) is only partially compensated by the lowering of electronic repulsion by the I···H to result in a minor stabilization relative to **ts4** (−5.5 kcal/mol).

3. Stabilization of Intermediates and Transition States through an Agostic Interaction. Two related types of metal–ligand association have been put forward as crucial in determining the energetics of the polytopal rearrangements. One interaction corresponds to the isomerization converting the ***endo*** complex to its ***exo-anti*** isomer, proceeding via **ts2**; the latter transition structure contains an incipient stabilizing C–H agostic interaction[22] that can decrease the barrier to octahedral **int2** (cf. Figure 2). Further analysis of the geometry of **int2** shows that the C–H bond involved in the agostic interaction undergoes significant elongation (1.18 Å) relative to the nonparticipating C–H bonds (1.10 Å).[23] Various Ru(II) complexes[2d,24] have indeed been shown to contain agostic interactions that, in some instances, result in C–H insertion.[25,26] An analogous association corresponds to a coordinatively unsaturated center being stabilized through an interaction with the Lewis basic π cloud of an aromatic ring.[25d] As depicted for **int0•H⁺** (Figure 5A), the

dx.doi.org/10.1021/ja410606b | J. Am. Chem. Soc. 2014, 136, 3439–3455

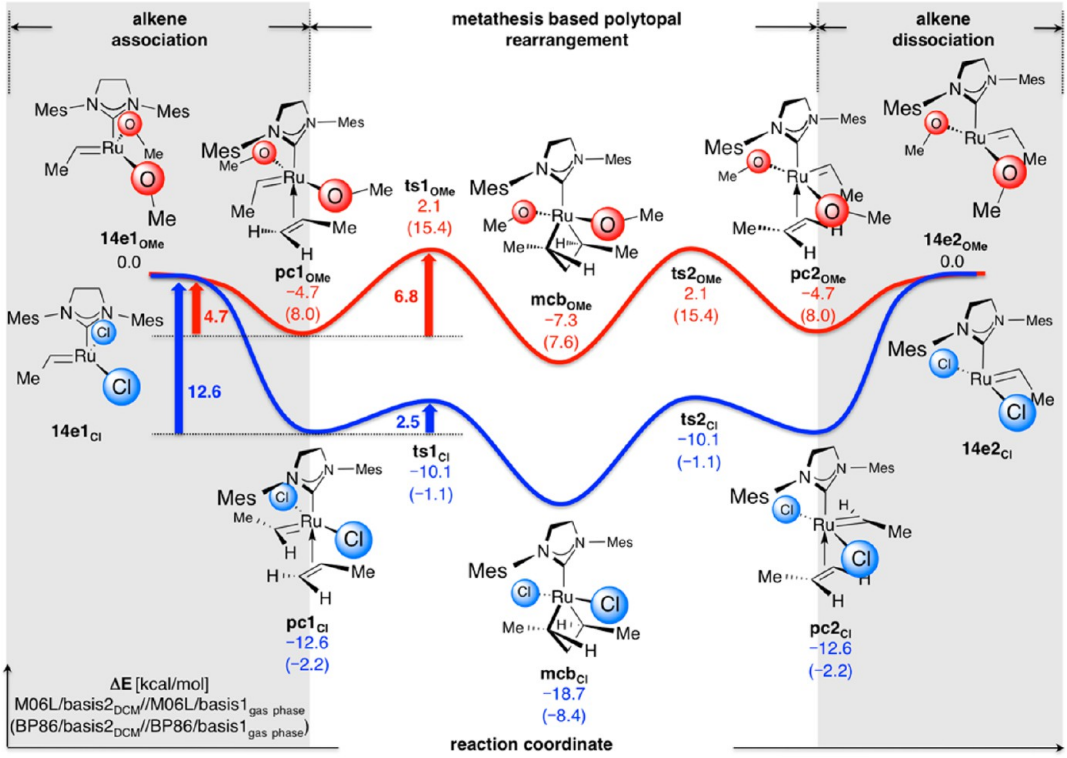

Figure 9. The effect of Cl (blue) and OMe (red) ligands on nonproductive CM with propene. Surface of the electronic energy (ΔE) referenced to 14e complexes in solution (dichloromethane) at the M06L/basis2 level of theory; values calculated with BP86/basis2 are in parentheses. pc = π complex, mcb = metallacyclobutane, ts = transition state.

same type of metal−ligand interaction might be at play when the ***endo*•H**$^+$ is transformed to the ***exo-syn*•H**$^+$ complex.

4. Mechanistic Implications Regarding the Role of Anionic Ligands on Olefin Metathesis Reactions and Catalyst Design. The investigations detailed above point to the critical role of anionic ligands within a Ru-based carbene complex in determining the facility with which polytopal rearrangements, whether OM-based or otherwise, proceed. Our investigations imply that examination of the mechanistic details of catalytic OM reactions or efforts toward designing efficient and stereoselective Ru-based complexes should take into account the influence of anionic ligands on the stability of the relevant transition states and intermediates. Below, we provide illustrative instances regarding a mechanistic investigation, a diastereoselective reaction development, and a catalyst design initiative.

4.1. Influence of Anionic Ligands on the Energetics of OM Reactions. Several investigations[27−31] have explored the structure−activity relationship of the first-[32,33] and second-generation[34,7] Ru complexes regarding the effect of the neutral phosphine[27a,35,2c−g] or NHC[36] units and that of anionic groups.[37] Substitution of the chlorides with other halides,[27] sulfonates,[2f,38] triflate,[39a] carboxylates,[2g,40] perfluorocarboxylates,[39−41] isocyanates,[39d,e] perhalophenolates,[42] nitrates,[2g,39e,10b] alkyl groups,[10] and thiolates[43] has been demonstrated to influence the rate of OM reactions. In most cases, a significant increase in reactivity has been observed for strongly σ-donating[28g,h,44] and sterically bulky[28d,h] NHC[45,46] and electron-withdrawing anion ligand combinations.[27,28i] In connection with the development of stereoselective complexes, however, the majority of efforts have been centered on steric modification of neutral (NHC) groups.[36,47,48] Catalyst development based on alteration of the anionic units has been less common, and it is only more recently that research efforts have resulted in identification of stereoselective Ru complexes where alteration of such ligands has played a critical role (cf. **4**−**6**, Scheme 2).[9,10,43a,49,2f]

To elucidate further the importance of anionic ligands, we chose to probe the details of a degenerate process involving a dimethoxide versus a dichloride complex.[50] Typically, in such instances, the diminished reactivity of Ru carbenes with the more strongly donating units (e.g., OMe) is attributed to the low binding affinity of a substrate.[51] The investigations detailed above show that there are other prominent electronic factors that originate from anionic units and impact reactivity and stereoselectivity. To highlight the fundamental similarities between non-OM-based polytopal rearrangement and OM, we set out to extend the orbital analysis originally put forth by Straub;[28i] the results of such studies are presented below.

The energy diagram for nonproductive CM involving propene in dichloromethane, a process that results in a side change of the carbene unit (**14e1**$_X$ → **14e2**$_X$; X = Cl, OMe), is presented in Figure 9.[18] We opted for the electronic energy (ΔE in kcal/mol) as the descriptor since it reflects the individual enthalpic contributions. Furthermore, we selected the M06-L functional[52] since it has been shown to reproduce bond dissociation energies more correctly due to superior treatment of noncovalent interactions (vs BP86, values for which appear in parentheses).[29b−d]

Analysis of the barriers associated with the potential energy surfaces indicates that alkene association/dissociation as well as OM-based rearrangement are energetically less favored with the stronger π-electron donating methoxide ligands. Binding of an alkene to the coordinatively unsaturated Ru-dimethoxide (**14e1**$_{OMe}$) is favored by −4.7 kcal/mol (red path, Figure 9),

dx.doi.org/10.1021/ja410606b | J. Am. Chem. Soc. 2014, 136, 3439−3455

affording π complex $\mathbf{pc1}_{\mathbf{OMe}}$ with a "vertical" carbene; here, the substituents are oriented toward the NHC and the bound propene (the term "inactive" has been previously used).[28i] Rotation of the Ru=C to the "horizontal" (or "active") form (substituents perpendicular to the NHC and the coordinated propene) followed by cycloaddition affords $\mathbf{mcb}_{\mathbf{OMe}}$. The sequence involving the dichloride complex (blue path, Figure 9) has several notable attributes. Alkene coordination is more exothermic (−12.6 kcal/mol), partly due to the higher energy LUMO (d_{z^2}) of $\mathbf{14e1}_{\mathbf{OMe}}$ and diminished Lewis acidity of the Ru-dimethoxide.[53] Furthermore, the Ru=C is horizontally disposed in $\mathbf{pc1}_{\mathbf{Cl}}$, ready for the cycloaddition that generates $\mathbf{mcb}_{\mathbf{Cl}}$, an intermediate that is significantly lower in energy than its dimethoxy counterpart ($\mathbf{mcb}_{\mathbf{OMe}}$). The low substrate binding affinity in the case of the Ru-dimethoxide species, combined with a higher barrier toward OM-based rearrangement ($\mathbf{pc1}_{\mathbf{OMe}} \rightarrow \mathbf{ts1}_{\mathbf{OMe}}$), result in an overall higher free energy barrier (ΔG in kcal/mol) compared to the Ru-dichloride (cf. Figure 10).[54]

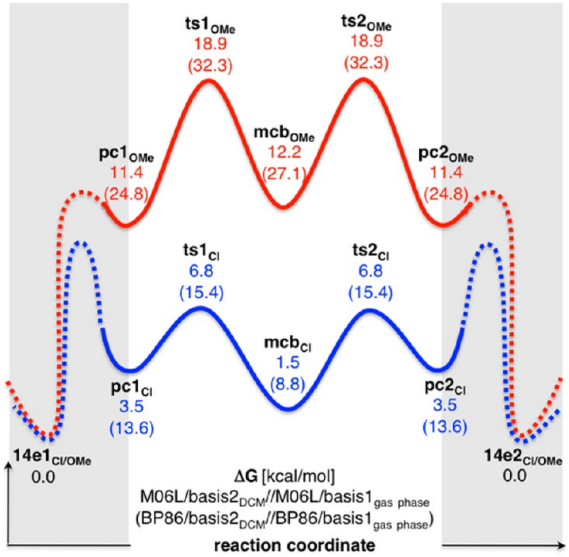

Figure 10. The effect of Cl (blue) and OMe (red) ligands on nonproductive CM with propene. Surface of the Gibbs free energy (ΔG) in solution (dichloromethane) referenced to 14e complexes at the M06-L/basis2 level of theory; values calculated with BP86/basis2 are in parentheses. pc = π complex, mcb = metallacyclobutane, ts = transition state.

The differences in the degree of donor−donor interactions as a function of the nature of the anionic ligands shed significant light on the origin of reactivity differences between the dichloro and bis-methoxide Ru complexes. Therefore, as a result of stronger trans influence, the MeO−Ru−OMe angle is smaller, a geometrical preference that, nonetheless, gives rise to electron−electron repulsion between the electrons in the p_z orbital on the alkoxides and those in the filled d_{xz} orbital. As has formerly been pointed out, alleviation of the latter destabilizing interactions can be achieved through π-back-donation, which is only feasible when the carbene adopts the vertical position so that its vacant p orbital is properly aligned (Figure 11b, right).[28i] Elongation of the Ru=C[55] upon olefin coordination ($\mathbf{pc1}_{\mathbf{OMe}}$) and its subsequent rotation into the necessary horizontal form needed for formation of $\mathbf{mcb}_{\mathbf{OMe}}$ diminishes π-back-donation. As a result, the repulsion involving the electrons in the Ru d_{xz} and those in the anion's p_z orbital increases; to curtail this unfavorable interaction, the MeO−Ru−OMe angle must expand (Figure 11b, left).[56] The latter adjustment elevates trans influence and repulsive π-donation involving the electrons in the p_x orbitals; this results in an elongation of the Ru−OMe bonds (Figure 11d) and substantial accumulation of charge on the alkoxide ligands (Figure 11e). The reason as to why the carbene prefers the vertical orientation in $\mathbf{pc1}_{\mathbf{OMe}}$ might be because steric repulsion between the bound alkene and the carbene substituent (Figure 11a) costs less than an increase in anionic donor−donor repulsion. It is for the same reason that formation of $\mathbf{mcb}_{\mathbf{OMe}}$ is more demanding, as it is accompanied by a substantial widening of the MeO−Ru−OMe angle (9.3°, Figure 11a and 11c).

The aforementioned trans influence is less severe in the case of less donating Cl ligands, which are better able to accommodate an increase of electron density. The Cl−Ru−Cl angle can therefore be more linear (blue curve in Figure 11c) and the Ru=C in $\mathbf{pc1}_{\mathbf{Cl}}$ can adopt the sterically less demanding horizontal form where the substituents point away from the sizable NHC or the bound alkene (Figures 9 and 11a). It is for these reasons that conversion of $\mathbf{pc1}_{\mathbf{Cl}}$ to $\mathbf{mcb}_{\mathbf{Cl}}$ demands a less significant expansion of the Cl−Ru−Cl angle (Figure 11a,c), a lower increase in Ru−Cl bond length (Figure 11d), and a smaller enhancement of charge accumulation on the anionic ligands (Figure 11e). Accordingly, more of the needed structural change en route to mcb formation takes place upon alkene coordination, rendering the subsequent cycloaddition step more facile.

The above analysis demonstrates that the influence of the anionic ligands within a Ru-based OM catalyst can be critical on several levels. Depending on the nature of anionic ligand, the rate-determing step can be altered from olefin association/dissociation to mcb formation/breakage (cf. Figure 10).

4.2. Electrostatic Interactions Involving Anionic Ligands and Ru-Catalyzed OM with Allylic Alcohols. The presence of an allylic substituent in an alkene substrate typically leads to significant attenuation of efficiency in catalytic OM. Such diminished reactivity might be the result of steric repulsion imposed by an adjacent secondary alkyl or aryl group or due to electronic deactivation imposed by a heteroatom-based substituent. It is thus anomalous that an allylic alcohol, even one that is tertiary, reacts at substantially faster rates and requires lower catalyst loadings.[57] Moreover, alcohol additives facilitate certain OM processes,[58] and the presence of acetic acid has been shown to accelerate RCM of diethyl diallylmalonate.[59]

A combination of two effects likely explains the above variations in reactivity: (1) Electrostatic attraction (H-bonding) between a chloride of the Ru complex and the substrate's hydroxyl group strengthens substrate binding (Scheme 6).[60] Inspired by the latter concept, a number of OM-based synthesis strategies have been successfully devised.[61] The hydroxyl-based electrostatic interactions probably have a similar origin as the Brønsted acid-catalyzed polytopal rearrangements. (2) Additionally, as illustrated in the representative case in Scheme 6, minimization of the destabilizing donor−donor interactions that probably exist between the two anionic chloride ligands in Ru−alkene complex **20** and mcb **21** might serve as the reason for the lowering of the barrier for the OM-based polytopal rearrangement. Furthermore, similar electrostatic associations can reduce the barrier to the CM step needed for efficient catalytic turnover, a principle manifested by conversion of intermediate **22** to ROCM product **25** via H-bonded complex **24**. Such stabilizing effects, promoted by relatively weak proton donors within a cross partner molecule, are sufficient to ease an OM process.

dx.doi.org/10.1021/ja410606b | J. Am. Chem. Soc. 2014, 136, 3439−3455

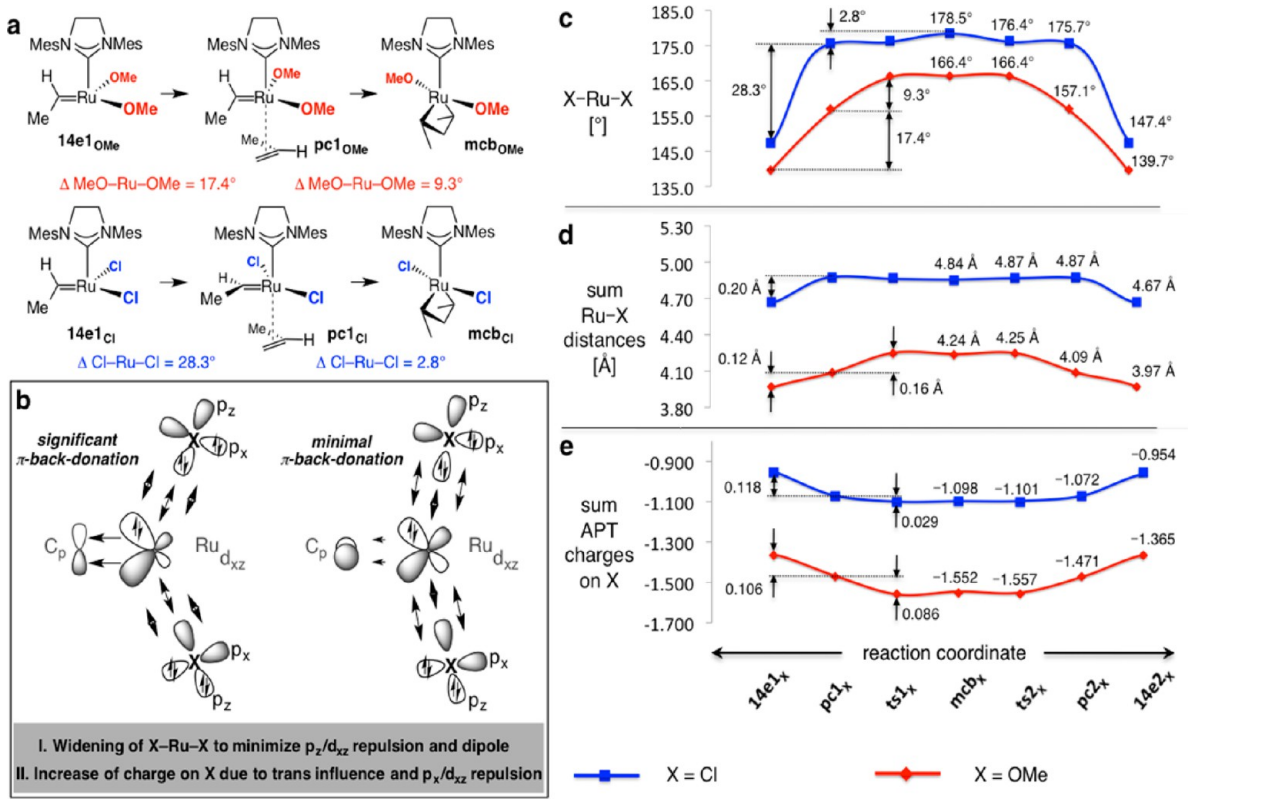

Figure 11. Evaluation of donor–donor interactions (BP86/basis1) that contribute to the energy barrier for the degenerate olefin metathesis from **14e1**$_X$ → **14e2**$_X$ through correlation of bond angles [deg] (c) and bond lengths [Å] (d) with the negative charge accumulation on the anionic ligands (e).

Scheme 6. Influence of H-Bonding on Ru-Catalyzed Diastereoselective ROCM Reaction

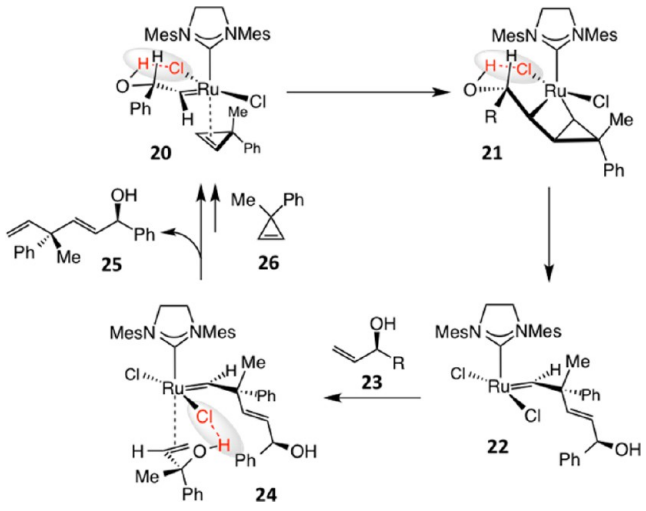

Scheme 7. Influence of Anionic Ligands on Alkene Association and Stereochemical Outcome of Olefin Metathesis Reactions

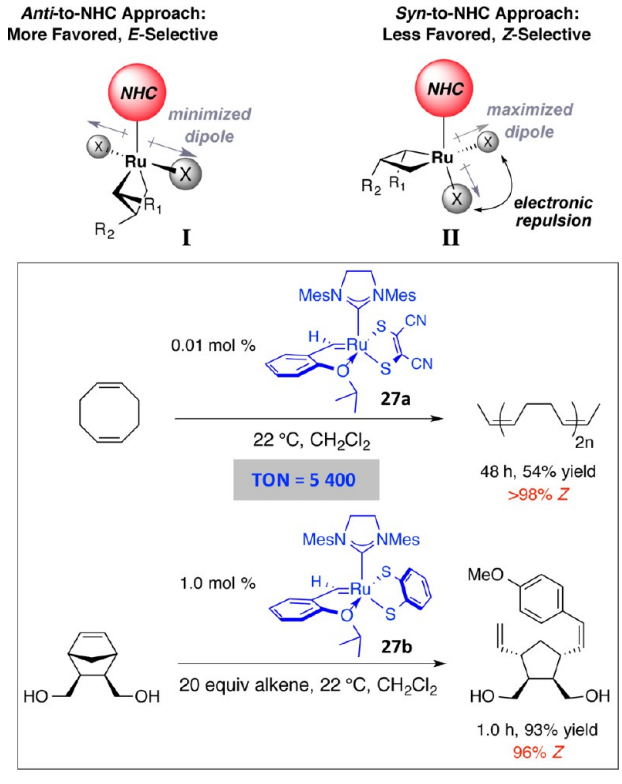

4.3. Design of Z-Selective Ru Catalysts through Manipulation of Anionic Ligands. Appreciation of the electronic effects arising from the highly polarized Ru–anion bonds and their influence in determining the facility with which OM reactions proceed is central to the design of stereoselective catalysts. The brief analysis provided below corresponds to two recent examples.

4.3.1. Enforcing Syn Orientation of Anionic Ligands by a Linker. Complex **I** in Scheme 7 represents the type of intermediates involved in the typically *E*-selective OM reactions promoted by the commonly used Ru dichloride catalysts.[48] As

dx.doi.org/10.1021/ja410606b | J. Am. Chem. Soc. 2014, 136, 3439–3455

previously indicated,[17,62] the preference for **I** is partly due to the destabilizing electron−electron repulsion and a large dipole moment in the alternative **II**, which is derived from olefin association[63] and cycloaddition syn to the NHC. Metallacycles represented by **II** possess the proper steric environment for generating *Z* alkenes.[49]

In designing a strategy that would favor the intermediacy of **II**, we evaluated the possibility of positioning an H-bond between the iodide and O^1 ligands in the hope that it would result in sufficient diminution of unfavorable dipolar effects involved in the conversion of ***14endo-anti*** to ***16exo-syn*** (via **ts2•H$^+$**; cf. Figure 8). We wondered whether similar electrostatic stabilization could influence the equilibrium between the two isomers **I** and **II** (Scheme 7) in favor of the latter. Eventually, we judged that the reduced propensity of a halide ligand to serve as the sole H-bond acceptor renders such an approach unfeasible (vs a proton bridge between a halide and phenoxide O^1 in Figure 8 or the hydroxyl group in Scheme 6).

We then envisaged that a covalent linker between the anionic ligands in **II** might offer a solution for overcoming the aforementioned unfavorable dipolar effects as well as provide a way for excluding the intermediacy of **I** (Scheme 7). We opted to replace the Cl atoms with a dithiolate unit (cf. **27a,b**, Scheme 7).[49] As the representative cases in Scheme 7 indicate, bis-sulfide complexes **27a** and **27b** promote efficient and exceptionally *Z*-selective ring-opening metathesis polymerization (ROMP) and ROCM reactions. In addition to underscoring the crucial role of anionic groups with a Ru complex, the latter advance highlights the positive influence of a covalent linker[64] between such ligands on *Z* selectivity.

4.3.2. Effect of Bidentate Anions on the Geometry d^6 Ru Carbene Complexes. A critical consequence of restricting the anionic ligands within a small ring structure is that the complex wherein the two negatively charged donor groups are syn to the NHC group is disfavored; hence, addition of an alkene anti to the NHC ligand is no longer possible. The basis for such a preference merits a brief discussion.

Achiral complexes such as Ru-dichlorides (e.g., **1**, Scheme 2) preferentially adopt an sp geometry, wherein the halide ligands are situated trans to one another and are syn to the NHC. In contrast, as illustrated in Scheme 8a, the small bite angle in the dithiolate group of **27b** (88.1°)[18] enforces a distorted sp geometry, wherein the sulfur atoms are forced to be syn with one residing trans to the N-heterocyclic moiety. The corresponding high-energy tbp system **28**, mentioned above, with both sulfide units positioned syn to the NHC, represents the higher energy transition state through which the enantiomers of the stereogenic-at-metal complex (***R*-27b** → ***S*-27b**) interconvert by a non-OM based polytopal rearrangement.

Why does a complex such as the tbp species **28** represent a transition state, while a dichloride Ru carbene, such as **1** or **2** (Scheme 2), corresponds to the lowest energy state?

In a d^6-RuL$_3$X$_2$ complex with a strongly σ-donating and π-accepting Ru=C the preferred electronic configuration is one where the $d_{x^2-y^2}$ orbital is unoccupied while the d_{xy} orbital is filled.[19] As illustrated in Scheme 8b (**III**), such an arrangement allows for efficient σ-donation of the electron density in the carbene's sp^2 orbital into the $d_{x^2-y^2}$, as well as efficient back-donation from the transition metal d_{xy} into Ru=C's p orbital (**IV**, Scheme 8b). The anionic halide ligands can establish a stabilizing overlap with the vacant $d_{x^2-y^2}$ orbital (cf. **III**, X = Cl). Equally noteworthy is that, as shown in **IV**, a lowering in the X−Ru−X angle results in a weak filled−filled interaction with the occupied d_{xy} orbital, enhancing back-donation with the carbene.[28i] In contrast, a significant reduction of the X−Ru−X angle through a small covalent linker, as is the case with **28** (88.2°), causes unfavorable electronic effects (see Scheme 8c).[18] Not only is the association of the bidentate dianionic ligand with the empty $d_{x^2-y^2}$ orbital nearly nonbonding (**V**, Scheme 8c), there is a destabilizing filled−filled interaction between the sulfide electrons and those in the occupied d_{xy} orbital (**VI**).[65] The latter factors combine to raise the energy of **28** by approximately 32 kcal/mol above that of **27b**.

Scheme 8. Effect of a Small Linker Between the Anionic Ligands on the Preferred Geometry of d^6 Ru Complexes

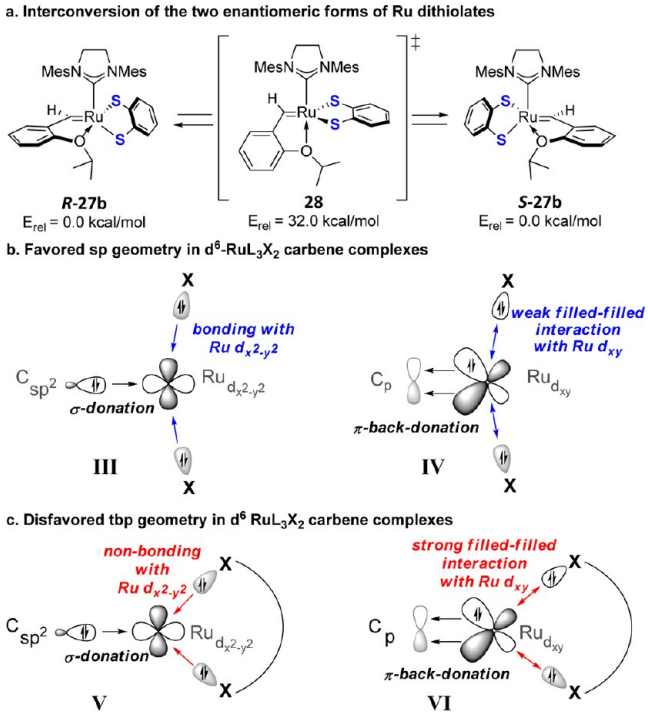

4.3.3. Relevance to Other Z-Selective Ru-Based Catalyst Systems. Unlike the aforementioned set of *Z*-selective dithiolate complexes, where anti-to-NHC approach is hindered by a sulfide ligand, in the reactions performed in the presence of Ru carbene **5** either syn- or anti-to-NHC mode approach is possible. As a result, the preference for the intermediacy of complex **VIII**, which accounts for the observed *Z* selectivities,[10c] versus the presumably *E* olefin generating **VII** (Scheme 9), might partly arise from electronic control through the anionic ligand.[50] As has been previously suggested, a pathway through **VIII** is favored due to a combination of several steric and electronic factors.[66] What is more, however, complementary factors that originate from the electron donating ability of the anionic ligands might be at work

Scheme 9. Electronic Differentiation between Syn-to-NHC and Anti-to-NHC Approach Induced by an Anionic Alkyl Ligand

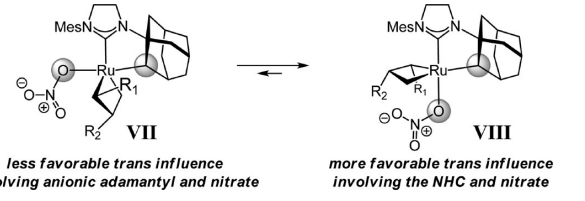

dx.doi.org/10.1021/ja410606b | J. Am. Chem. Soc. 2014, 136, 3439−3455

as well. It is likely that complex **VII**, the intermediate leading to the to *E*-alkene products, is less preferred since it suffers from trans influence involving the nitrate and the strongly donating anionic adamantyl ligand. In the mode of reaction (**VIII**) that results in the formation of the *Z* isomer, it is the less strongly donating neutral NHC (vs carbanionic) ligand that resides opposite to the O-based unit.

CONCLUSIONS

The investigations detailed in this report highlight the importance of an assortment of factors associated with the anionic ligands that govern polytopal rearrangements of Ru-based carbene complexes. Detailed DFT analysis of thermally induced as well as Brønsted acid-catalyzed non-OM-based polytopal interconversion of Ru complex **14*endo-anti*** to **17*exo-anti*** (cf. Scheme 4) provide the following insights and rationales for several experimental findings:

(1) Isolation of the high-energy but kinetically stable Ru complex **14*endo-anti*** is due to unfavorable interactions within intermediates and transition states that this entity faces en route to a lower energy isomer; the energetically costly associations stem largely from the influence of the anionic ligands. Such hurdles are overcome at 60 °C to afford the thermodynamically preferred **17*exo-anti***.

(2) Significant donor−donor interactions in Ru-based carbenes engendered by anionic ligands are revealed through correlation of the negative charge accumulation upon the change in geometric parameters (e.g., trans relationship). Such analyses point to unfavorable charge accrual on the iodide and phenoxide ligands (O^1) when positioned opposite to the electron-donating carbene groups [i.e., C^1 (NHC) and alkylidene C^2 in Figure 7].

(3) The increase in the dipole moment of intermediates and transition states in the course of polytopal rearrangements originates from the tightening of the angle between the two anionic groups (Figure 8) and results in an increase in charge repulsion. These destabilizing structural and electronic alterations (listed above in points 2 and 3) accumulate in the rate-determining transition state for the thermally promoted isomerization (cf. **ts2**, Figure 1).

(4) Analysis of the potential energy surface for rearrangement of Ru complex ***endo*** versus ***endo*•H$^+$** points to a significant minimization of donor−donor interactions and dipole moments in the ensuing structures involved in the polytopal rearrangement. The presence of the Lewis acid alters the rate-determining step from transition state **ts2** to **ts4•H$^+$** (Figure 4), such that the metastable intermediate **16*exo-syn*** becomes isolable (cf. Scheme 4).

(5) Accumulation of electron density on the anionic phenoxide ligand (O^1) in transition complex **ts2** is compensated by the acid additive, resulting in diminished donor−donor interaction with the alkylidene C^2; this is reflected in the lengthening of the Ru−O^1 bond (Figure 7).

(6) The high dipole moment in **ts2**, which arises from charge repulsion between the two anionic ligands (I and O^1), is minimized due to protonation and formation of **ts2•H$^+$**. This is indicated by an additional H-bond between the iodide and the phenoxide ligands leading to tightening of the I−Ru−O^1 angle (Figure 8).

(7) Unlike the influence of a Brønsted acid on isomerization of **14*endo-anti*** to **16*exo-syn***, partly emanating from the differences between **ts2** and **ts2•H$^+$**, protonation of **ts4** has little impact on the rate of conversion of **16*exo-syn*** to **17*exo-anti***. Such dissimilarity in the influence exerted by the protic acid allows for isolation of **16*exo-syn*** as the exclusive product upon treatment of high energy but kinetically stable **14*endo-anti*** with HOAc. Heating of **16*exo-syn*** leads to the lowest energy complex **17*exo-anti***.

The impact of anionic ligands and control of electronic forces that is a consequence of their presence has led to a number of mechanistic insights and successful development of *Z*-selective Ru-based catalysts. Specifically, the following principles should be underscored:

(1) The improved activity of Ru dichlorides versus the bis-methoxides originates from the unfavorable trans relationship of the more strongly electron donating methoxide ligands (vs Cl). The impact of anionic units (X = Cl vs OMe) in second-generation Ru systems on the barrier for nonproductive OM with propene (Figures 9 and 10) exhibits an analogous correlation of geometric parameters (i.e., X−Ru−X bond angles) with negative charge build-up on the said ligands (Figure 11).

(2) In line with the lower barriers associated with the non-OM-based rearrangement in the presence of a Lewis acidic proton, the effect of H-bonding on efficiency of OM reactions with allylic alcohols can be accounted for.

(3) An exceptionally *Z*-selective Ru-based catalyst has been developed by way of manipulation of anionic ligands so that unfavorable dipole−dipole interactions and electron−electron repulsive forces are countered, obviating the anti-to-NHC olefin approach and mcb formation that results in *E*-selective processes. A sulfur-based dianionic ligand was incorporated into the catalyst structure to enforce the syn-to-NHC mode of mcb production, resulting in high *Z* selectivity. Related effects involving anionic ligands play a seminal function in the effectiveness of another class of *Z*-selective Ru-based OM catalysts.

Design and development of efficient and stereoselective OM catalysts based on the mechanistic principles and insights described above are in progress in these laboratories.

ASSOCIATED CONTENT

Supporting Information

Geometries and energies of computed structures, tables including structural parameters (bond lengths and angles) and electronic charges (APT-charges and those obtained through Bader charge analysis), three-dimensional energy diagrams of potential energy surfaces obtained from IRC (intrinsic reaction coordinate) calculations as well as an animation of the thermally induced polytopal rearrangement, shown in Figure 1, and the analysis of frontier Kohn−Sham orbitals for 14-electron and mcb complexes as a function of the donor ability of anionic ligands (Cl vs OMe). This material is available free of charge via the Internet at http://pubs.acs.org.

AUTHOR INFORMATION

Corresponding Author

amir.hoveyda@bc.edu

Author Contributions

‡S.T. and R.K.M.K. contributed equally to this research.

Notes

The authors declare no competing financial interest.

ACKNOWLEDGMENTS

Financial support was provided by the NSF (CHE-1111074). S.T. and R.K.M.K. were partially supported by Swiss NSF Postdoctoral and LaMattina Fellowships. Helpful discussions

with Adil R. Zhugralin are acknowledged. We thank Boston College Research Services for access to computational facilities.

REFERENCES

(1) (a) Hoveyda, A. H.; Zhugralin, A. R. *Nature* **2007**, *450*, 243−251. (b) Fürstner, A. *Science* **2013**, *341*, 1357−1364.

(2) The concept of a side change of a carbene unit in a Ru-based complex was initially suggested by Chen and co- workers as part of their kinetic isotope effect studies, which were performed in the gas phase. See: (a) Adlhart, C.; Hinderling, C.; Baumann, H.; Chen, P. *J. Am. Chem. Soc.* **2000**, *122*, 8204−8214. (b) Adlhart, C.; Chen, P. *Angew. Chem., Int. Ed.* **2002**, *41*, 4484−4487. This feature was later applied in the development of a chemoselective Ru-based catalyst for alternating copolymerization: (c) Bornand, M.; Chen, P. *Angew. Chem., Int. Ed.* **2005**, *44*, 7909−7911. (d) Bornand, M.; Torker, S.; Chen, P. *Organometallics* **2007**, *26*, 3585−3596. (e) Torker, S.; Müller, A.; Sigrist, R.; Chen, P. *Organometallics* **2010**, *29*, 2735−2751. (f) Torker, S.; Müller, A.; Chen, P. *Angew. Chem., Int. Ed.* **2010**, *49*, 3762−3766. (g) Jovic, M.; Torker, S.; Chen, P. *Organometallics* **2011**, *30*, 3971−3980. (h) Bornand, M.; Torker, S.; Chen, P. *Polym. Prepr.* **2011**, *52*, 214−215.

(3) Khan, R. K. M.; Zhugralin, A. R.; Torker, S.; O'Brien, R. V.; Lombardi, P. J.; Hoveyda, A. H. *J. Am. Chem. Soc.* **2012**, *134*, 12438−12441.

(4) For recent reviews on polytopal rearrangements in pentacoordinated complexes, see: (a) Couzijn, E. P. A.; Slootweg, J. C.; Ehlers, A. W.; Lammertsma, K. *J. Am. Chem. Soc.* **2010**, *132*, 18127−18140. (b) Moberg, C. *Angew. Chem., Int. Ed.* **2011**, *50*, 10290−10292.

(5) For early work on the mechanism of polytopal rearrangements, see: (a) Berry, R. S. *J. Chem. Phys.* **1960**, *32*, 933−938. (b) Mutterties, E. L. *J. Am. Chem. Soc.* **1969**, *91*, 1636−1643. (c) Gillespie, P.; Hoffman, P.; Klusacek, H.; Marquarding, D.; Phohl, S.; Ramirez, F.; Tsolis, E. A.; Ugi, I. *Angew. Chem., Int. Ed. Engl.* **1971**, *10*, 687−715.

(6) Polytopal rearrangement in a pentacoordinated molybdacyclobutane structure has been envoked to occur during the synthesis of highly trans, highly isotactic ROMP polymers from norbornadiene derivatives: Flook, M. M.; Börner, J.; Kilyanek, S. M.; Gerber, L. C. H.; Schrock, R. R. *Organometallics* **2012**, *31*, 6231−6243.

(7) Garber, S. B.; Kingsbury, J. S.; Gray, B. L.; Hoveyda, A. H. *J. Am. Chem. Soc.* **2000**, *122*, 8168−8179.

(8) Funk, T. W.; Berlin, J. M.; Grubbs, R. H. *J. Am. Chem. Soc.* **2006**, *128*, 1840−1846.

(9) For applications of enantiomerically enriched stereogenic-at-Ru carbene complexes in chemical synthesis, see: (a) Van Veldhuizen, J. J.; Garber, S. B.; Kingsbury, J. S.; Hoveyda, A. H. *J. Am. Chem. Soc.* **2002**, *124*, 4954−4955. (b) Van Veldhuizen, J. J.; Gillingham, D. G.; Garber, S. B.; Kataoka, O.; Hoveyda, A. H. *J. Am. Chem. Soc.* **2003**, *125*, 12502−12508. (c) Gillingham, D. G.; Kataoka, O.; Garber, S. B.; Hoveyda, A. H. *J. Am. Chem. Soc.* **2004**, *126*, 12288−12290. (d) Van Veldhuizen, J. J.; Campbell, J. E.; Giudici, R. E.; Hoveyda, A. H. *J. Am. Chem. Soc.* **2005**, *127*, 6877−6882. (e) Gillingham, D. G.; Hoveyda, A. H. *Angew. Chem., Int. Ed.* **2007**, *46*, 3860−3864.

(10) For a representative list of applications of stereogenic-at-Ru complexes that contain a chelated alkyl donor ligand, see: (a) Endo, K.; Grubbs, R. H. *J. Am. Chem. Soc.* **2011**, *133*, 8525−8527. (b) Keitz, B. K.; Endo, K.; Patel, P. R.; Herbert, M. B.; Grubbs, R. H. *J. Am. Chem. Soc.* **2012**, *134*, 693−699. (c) Liu, P.; Xu, X.; Dong, X.; Keitz, B. K.; Herbert, M. B.; Grubbs, R. H.; Houk, K. N. J. *Am. Chem. Soc* **2012**, *134*, 1464−1467. (d) Marx, V. M.; Herbert, M. B.; Keitz, B. K.; Grubbs, R. H. *J. Am. Chem. Soc.* **2013**, *135*, 94−97. (e) Herbert, M. B.; Marx, V. M.; Pederson, R. L.; Grubbs, R. H. *Angew. Chem., Int. Ed.* **2013**, *52*, 310−314. (f) Rosebrugh, L. E.; Herbert, M. B.; Marx, V. M.; Keitz, B. K.; Grubbs, R. H. *J. Am. Chem. Soc.* **2013**, *135*, 1276−1279. (g) Rosebrugh, L. E.; Marx, V. M.; Keitz, B. K.; Grubbs, R. H. *J. Am. Chem. Soc.* **2013**, *135*, 10032−10035. (h) Hartung, J.; Grubbs, R. H. *J. Am. Chem. Soc.* **2013**, *135*, 10183−10185.

(11) For alternative enantiomerically pure stereogenic-at-Mo OM catalysts and their application in chemical synthesis, see: (a) Malcolmson, S. J.; Meek, S. J.; Sattely, E. S.; Schrock, R. R.; Hoveyda, A. H. *Nature* **2008**, *456*, 933−937. (b) Ibrahem, I.; Yu, M.; Schrock, R. R.; Hoveyda, A. H. *J. Am. Chem. Soc.* **2009**, *131*, 3844−3845. (c) Meek, S. J.; O'Brien, R. V.; Llaveria, J.; Schrock, R. R.; Hoveyda, A. H. *Nature* **2011**, *471*, 461−466. (d) Yu, M.; Ibrahem, I.; Hasegawa, M.; Schrock, R. R.; Hoveyda, A. H. *J. Am. Chem. Soc.* **2012**, *134*, 2788−2799. (e) Kiesewetter, E. T.; O'Brien, R. V.; Yu, E. C.; Meek, S. J.; Schrock, R. R.; Hoveyda, A. H. *J. Am. Chem. Soc.* **2013**, *135*, 6026−6029. (f) Mann, T. J.; Speed, A. W. H.; Schrock, R. R.; Hoveyda, A. H. *Angew. Chem., Int. Ed.* **2013**, *52*, 8395−8400. For investigations involving stereogenic-at-W complexes, see: (g) Yu, M.; Wang, C.; Kyle, A. F.; Jakubec, P.; Dixon, D. J.; Schrock, R. R.; Hoveyda, A. H. *Nature* **2011**, *479*, 88−93. (h) Townsend, E. M.; Schrock, R. R.; Hoveyda, A. H. *J. Am. Chem. Soc.* **2012**, *134*, 11334−11337. (i) Wang, C.; Yu, M.; Kyle, A. F.; Jakubec, P.; Dixon, D. J.; Schrock, R. R.; Hoveyda, A. H. *Chem.—Eur. J.* **2013**, *19*, 2726−2740.

(12) Herisson, J. L.; Chauvin, Y. *Makromol. Chem.* **1971**, *141*, 161−176.

(13) Khan, R. K. M.; O'Brien, R. V.; Torker, S.; Hoveyda, A. H. *J. Am. Chem. Soc.* **2012**, *134*, 12774−12779.

(14) (a) Kavitake, S.; Samantaray, M. K.; Dehn, R.; Deuerlein, S.; Limbach, M.; Schachner, J. A.; Jeanneau, E.; Coperet, C.; Thieuleux, C. *Dalton Trans.* **2011**, *40*, 12443−12446. Further work has invoked a mechanism through chain-end control for selective discrimination between chemically and sterically distinict olefins: (b) Vehlow, K.; Wang, D.; Buchmeiser, M. R.; Blechert, S. *Angew. Chem., Int. Ed.* **2008**, *47*, 2615−2618. (c) Lichtenheldt, M.; Wang, D.; Vehlow, K.; Reinhardt, I.; Kühnel, C.; Decker, U.; Blechert, S.; Buchmeiser, M. R. *Chem.—Eur. J.* **2009**, *15*, 9451−9457.

(15) Earlier investigations of non-OM-based polytopal rearrangements have focused on Type I complexes. These studies point to a dependence of the cis/trans equilibrium in dichloride complexes on the donor ability of chelated or monodentate neutral ligands (e.g., chelated isopropoxy group in complex **1**). See: (a) Ung, T.; Hejl, A.; Grubbs, R. H.; Schrodi, Y. *Organometallics* **2004**, *23*, 5399−5401. (b) Slugovc, C.; Perner, B.; Stelzer, F.; Mereiter, K. *Organometallics* **2004**, *23*, 3622−3626. (c) Zirngast, M.; Pump, E.; Leitgeb, A.; Albering, J. H.; Slugovc, C. *Chem. Commun.* **2011**, *47*, 2261−2263. (d) Leitgeb, A.; Mereiter, K.; Slugovc, C. *Monatsh. Chem.* **2012**, *143*, 901−908. (e) Pump, E.; Fischer, R. C.; Slugovc, C. *Organometallics* **2012**, *31*, 6972−6979. (f) Barbasiewicz, M.; Szadkowska, A.; Bujok, R.; Grela, K. *Organometallics* **2006**, *25*, 3599−3604. (g) Gstrein, X.; Burtscher, D.; Szadkowska, A.; Barbasiewicz, M.; Stelzer, F.; Grela, K.; Slugovc, C. *J. Polym. Sci., Part A: Polym. Chem.* **2007**, *45*, 3494. (h) Barbasiewicz, M.; Michalak, M.; Grela, K. *Chem.—Eur. J.* **2012**, *18*, 14237−14241. (i) Barbasiewicz, M.; Krzysztof, B.; Malinska, M.; Pawlowski, R. *Dalton Trans.* **2013**, *42*, 355−358. (j) Ben-Asuly, A.; Tzur, E.; Diesendruck, C. E.; Sigalov, M.; Goldberg, I.; Lemcoff, G. N. *Organometallics* **2008**, *27*, 811−813. (k) Diesendruck, C. E.; Tzur, E.; Ben-Asuly, A.; Goldberg, I.; Straub, B. F.; Lemcoff, N. G. *Inorg. Chem.* **2009**, *48*, 10819−10825. (l) Tzur, E.; Szadkowska, A.; Ben-Asuly, A.; Makal, A.; Goldberg, I.; Wozniak, K.; Grela, K.; Lemcoff, N. G. *Chem.—Eur. J.* **2010**, *16*, 8726−8737. (m) Aharoni, A.; Vidavsky, Y.; Diesendruck, C. E.; Ben-Asuly, A.; Goldberg, I.; Lemcoff, N. G. *Organometallics* **2011**, *30*, 1607−1615. (n) Bantreil, X.; Schmid, T. E.; Randall, R. A. M.; Slawin, A. M. Z.; Cazin, C. S. J. *Chem. Commun.* **2010**, *46*, 7115−7117. (o) Schmid, T. E.; Bantreil, X.; Citadelle, C. A.; Slawin, A. M. Z.; Cazin, C. S. J. *Chem. Commun.* **2011**, *47*, 7060−7062.

(16) For a computational study regarding the reaction pathway for the cis/trans isomerization reported in ref 15f, see: Poater, A.; Ragone, F.; Correa, A.; Szadkowska, A.; Barbasiewicz, M.; Grela, K.; Cavallo, L. *Chem.—Eur. J.* **2010**, *16*, 14354−14364.

(17) For a computational investigation of solvent effects on the cis/trans equilibrium reported in ref 15a, see: Benitez, D.; Goddard, W. A. *J. Am. Chem. Soc.* **2005**, *127*, 12218−12219.

(18) Unless otherwise noted, calculations and structural analyses have been performed with Gaussian 09 in gas phase at the BP86/basis1 level of theory. In the explicitly mentioned cases, additional structure optimizations in gas phase with basis1 have been performed with functionals that have been corrected for the treatment of dispersion

interactions (ωB97XD, M06, and M06-L), followed by single point energy calculations in solution through the use of either basis1 or the larger basis2. For further computational details and definition of basis sets, see the Supporting Information.

(19) For a discussion of the geometry of d^6 ML_5 complexes containing either π-accepting or π-donating ligands, see: Riehl, J.-F.; Jean, Y.; Eisenstein, O.; Pelissier, M. *Organometallics* **1992**, *11*, 729−737.

(20) Further insight regarding the mechanism of the aforementioned rearrangement (concerted or stepwise bond angle variations) is provided through three-dimensional visualization of the potential energy surface, obtained from IRC (intrinsic reaction coordinate) calculations. See the Supporting Information for details.

(21) For a computational study of the energetics of the Ru−halide bond in OM catalysts, see: Falivene, L.; Poater, A.; Cazin, C. S. J.; Slugovc, C.; Cavallo, L. *Dalton Trans.* **2013**, *42*, 7312−7317.

(22) For a review on C−H agostic interactions, see: Crabtree, R. H. *Angew. Chem., Int. Ed.* **1993**, *32*, 789−805.

(23) Calculations on a model system, which lacks the *o*-methyl groups (denoted with subscript *o*-H), have been performed to probe the role of *o*-methyl groups in stabilizing the empty coordination site in **int2** (see the Supporting Information for details). Similar to the results described in Figure 1, polytopal rearrangement of the further truncated system (***endo***$_{o\text{-H}}$ → ***exo-anti***$_{o\text{-H}}$) progresses through analogous intermediates and transition states. In **int2**$_{o\text{-H}}$ the aromatic C−H bond appears to be involved in an agostic interaction as evident by the significant elongation to 1.20 Å, rendering **int2**$_{o\text{-H}}$ (E_{rel} = 13.7 kcal/mol) even more stable than **int2** (E_{rel} = 23.4 kcal/mol). The latter observation is in agreement with the greater propensity of Ru-complexes bearing NHC ligands with unsubstituted phenyl rings to undergo C−H activation, ultimately leading to their reduced stability.

(24) For representative noncarbene Ru(II) complexes, see: (a) Huang, D.; Huffman, J. C.; Bollinger, J. C.; Eisenstein, O.; Caulton, K. G. *J. Am. Chem. Soc.* **1997**, *119*, 7398−7399. (b) Huang, D.; Streib, W. E.; Bollinger, J. C.; Caulton, K. G.; Winter, R. F.; Scheiring, T. *J. Am. Chem. Soc.* **1999**, *121*, 8087−8097. (c) Huang, D.; Bollinger, J. C.; Streib, W. E.; Folting, K.; Young, V., Jr.; Eisenstein, O.; Caulton, K. G. *Organometallics* **2000**, *19*, 2281−2290. (d) Baratta, W.; Herdtweck, E.; Rigo, P. *Angew. Chem., Int. Ed.* **1999**, *39*, 1629−1632. (e) Scott, N. M.; Dorta, R.; Stevens, E. D.; Correa, A.; Cavallo, L.; Nolan, S. P. *J. Am. Chem. Soc.* **2005**, *127*, 3516−3526.

(25) (a) Vehlow, K.; Gessler, S.; Blechert, S. *Angew. Chem., Int. Ed.* **2007**, *46*, 8082−8085. (b) Endo, K.; Grubbs, R. H. *J. Am. Chem. Soc.* **2011**, *133*, 8525−8527. (c) Leitao, E. M.; Dubberley, S. R.; Piers, W. E.; Wu, Q.; McDonald, R. *Chem.—Eur. J.* **2008**, *14*, 11565−11572. (d) Hong, S. H.; Chlenov, A.; Day, M. W.; Grubbs, R. H. *Angew. Chem., Int. Ed.* **2007**, *46*, 5148−5151.

(26) A similar type of σ-type ligation has been implicated in a number of organometallic complexes, the most celebrated of which are those involved in Zielger−Natta olefin polymerization processes. See: (a) Krauledat, H.; Brintzinger, H. H. *Angew. Chem., Int. Ed. Engl.* **1990**, *29*, 1412−1413. (b) Piers, W. E.; Bercaw, J. E. *J. Am. Chem. Soc.* **1990**, *112*, 9406−9407. (c) Clawson, L.; Soto, J.; Buchwald, S. L.; Steigerwald, M. L.; Grubbs, R. H. *J. Am. Chem. Soc.* **1985**, *107*, 3377−3378.

(27) (a) Dias, E. L.; Nguyen, S. T.; Grubbs, R. H. *J. Am. Chem. Soc.* **1997**, *119*, 3887−3897. (b) Sanford, M. S.; Love, J. A.; Grubbs, R. H. *J. Am. Chem. Soc.* **2001**, *123*, 6543−6554.

(28) For experimental studies regarding the activity of first- versus second-generation Ru complexes in solution and gas phase, see: (a) Ref 27b. (b) Adlhart, C.; Chen, P. *Helv. Chim. Acta* **2003**, *86*, 941−949. For the corresponding theoretical studies, see: (c) Vyboishchikov, S. F.; Bühl, M.; Thiel, W. *Chem.—Eur. J.* **2002**, *8*, 3962−3975. (d) Cavallo, L. *J. Am. Chem. Soc.* **2002**, *124*, 8965−8973. (e) Adlhart, C.; Chen, P. *J. Am. Chem. Soc.* **2004**, *126*, 3496−3510. (f) Tsipis, A. C.; Orpen, A. G.; Harvey, J. N. *Dalton Trans.* **2005**, 2849−2858. (g) Straub, B. F. *Angew. Chem., Int. Ed.* **2005**, *44*, 5974−5978. (h) Occhipinti, G.; Bjorsvik, H. R.; Jensen, V. R. *J. Am. Chem. Soc.* **2006**, *128*, 6952−6964. (i) Straub, B. F. *Adv. Synth. Catal.* **2007**, *349*, 204−214. (j) Mathew, J.; Suresh, C. H. *Organometallics* **2011**, *30*, 1438−1444. (k) Mathew, J.; Suresh, C. H. *Organometallics* **2011**, *30*, 3106−3112. (l) Minenkov, Y.; Occhipinti, G.; Jensen, V. R. *Organometallics* **2013**, *32*, 2099−2111.

(29) For experimental studies regarding the relative initiation rates (phosphine dissociation) of first- vs second-generation Ru complexes in solution and gas phase, see: (a) Ref 27b. (b) Torker, S.; Merki, D.; Chen, P. *J. Am. Chem. Soc.* **2008**, *130*, 4808−4814. For recent theoretical studies, see: (c) Zhao, Y.; Truhlar, D. G. *Org. Lett.* **2007**, *9*, 1967−1970. (d) Minenkov, Y.; Occhipinti, G.; Jensen, V. R. *J. Phys. Chem. A* **2009**, *113*, 11833−11844. (e) Yang, H. C.; Huang, Y. C.; Lan, Y. K.; Luh, T. Y.; Zhao, Y.; Truhlar, D. G. *Organometallics* **2011**, *30*, 4196−4200. (f) Minenkov, Y.; Occhipinti, G.; Heyndrickx, W.; Jensen, V. R. *Eur. J. Inorg. Chem.* **2012**, 1507−1516. (g) Urbina-Blanco, C. A.; Poater, A.; Lebl, T.; Manzini, S.; Slawin, A. M. Z.; Cavallo, L.; Nolan, S. P. *J. Am. Chem. Soc.* **2013**, *135*, 7073−7079.

(30) (a) Eisenstein, O.; Hoffmann, R.; Rossi, A. R. *J. Am. Chem. Soc.* **1981**, *103*, 5582−5584. (b) Suresh, C. H.; Koga, N. *Organometallics* **2004**, *23*, 76−80. (c) Suresh, C. H.; Baik, M. H. *Dalton Trans.* **2005**, 2982−2984.

(31) For mechanistic studies regarding spectroscopic characterization of ruthenacyclobutane intermediates, see: (a) Romero, P. E.; Piers, W. E. *J. Am. Chem. Soc.* **2005**, *127*, 5032−5033. (b) Wenzel, A. G.; Grubbs, R. H. *J. Am. Chem. Soc.* **2006**, *128*, 16048−16049. (c) Romero, P. E.; Piers, W. E. *J. Am. Chem. Soc.* **2007**, *129*, 1698−1704. (d) van der Eide, E. F.; Romero, P. E.; Piers, W. E. *J. Am. Chem. Soc.* **2008**, *130*, 4485−4491. (e) van der Eide, E. F.; Piers, W. E. *Nat. Chem.* **2010**, *2*, 571−576. (f) Wenzel, A. G.; Blake, G.; VanderVelde, D. G.; Grubbs, R. H. *J. Am. Chem. Soc.* **2011**, *133*, 6429−6439.

(32) Schwab, P.; Grubbs, R. H.; Ziller, J. W. *J. Am. Chem. Soc.* **1996**, *118*, 100−110.

(33) Kingsbury, J. S.; Harrity, J. P. A.; Bonitatebus, P. J.; Hoveyda, A. H. *J. Am. Chem. Soc.* **1999**, *121*, 791−799.

(34) (a) Huang, J.; Stevens, E. D.; Nolan, S. P.; Peterson, J. L. *J. Am. Chem. Soc.* **1999**, *121*, 2674−2678. (b) Scholl, M.; Ding, S.; Lee, C. W.; Grubbs, R. H. *Org. Lett.* **1999**, *1*, 953−956. (c) Weskamp, T.; Kohl, F. J.; Hieringer, W.; Gliech, D.; Herrmann, W. A. *Angew. Chem., Int. Ed.* **1999**, *38*, 2416−2419.

(35) (a) Forman, G. S.; McConnell, A. E.; Hanton, M. J.; Slawin, A. M. Z.; Tooze, R. P.; van Rensburg, W. J.; Meyer, W. H.; Dwyer, C.; Kirk, M. M.; Serfontein, D. W. *Organometallics* **2004**, *23*, 4824−4827. (b) van Rensburg, W. J.; Steynberg, P. J.; Kirk, M. M.; Meyer, W. H.; Forman, G. S. *J. Organomet. Chem.* **2006**, *691*, 5312−5325.

(36) For a review on Ru-based complexes with an NHC ligand, see: Vougioukalakis, G. C.; Grubbs, R. H. *Chem. Rev.* **2010**, *110*, 1746−1787.

(37) For a review regarding bidentate LX-type ligands used in latent olefin metathesis catalysts, see: Monsaert, S.; Vila, A. L.; Drozdzak, R.; Van Der Voort, P.; Verpoort, F. *Chem. Soc. Rev.* **2009**, *38*, 3360−3372.

(38) Teo, P.; Grubbs, R. H. *Organometallics* **2010**, *29*, 6045−6050.

(39) (a) Krause, J. O.; Nuyken, O.; Wurst, K.; Buchmeiser, M. R. *Chem.—Eur. J.* **2004**, *10*, 777−784. (b) Halbach, T. S.; Mix, S.; Fischer, D.; Maechling, S.; Krause, J. O.; Sievers, C.; Blechert, S.; Nuyken, O.; Buchmeiser, M. R. *J. Org. Chem.* **2005**, *70*, 4687−4694. (c) Vehlow, K.; Maechling, S.; Köhler, K.; Blechert, S. *Tetrahedron Lett.* **2006**, *47*, 8617−8620. (d) Kumar, P. S.; Wurst, K.; Buchmeiser, M. R. *Chem.—Asian J.* **2009**, *4*, 1275−1283. (e) Buchmeiser, M. R.; Ahmad, I.; Gurram, V.; Kumar, P. S. *Macromolecules* **2011**, *44*, 4098−4106.

(40) Buchowicz, W.; Ingold, F.; Mol, J. C.; Lutz, M.; Spek, A. L. *Chem.—Eur. J.* **2001**, *7*, 2842−2847.

(41) Wu, Z.; Nguyen, S. T.; Grubbs, R. H.; Ziller, J. W. *J. Am. Chem. Soc.* **1995**, *117*, 5503−5511.

(42) (a) Conrad, J. C.; Amoroso, D.; Czechura, P.; Yap, G. P. A.; Fogg, D. E. *Organometallics* **2003**, *22*, 3634−3636. (b) Conrad, J. C.; Parnas, H. H.; Snelgrove, J. L.; Fogg, D. E. *J. Am. Chem. Soc.* **2005**, *127*, 11882−11883.

(43) (a) Occhipinti, G.; Hansen, F. R.; Törnroos, K. W.; Jensen, V. R. *J. Am. Chem. Soc.* **2013**, *135*, 3331−3334. (b) McKinty, A. M.; Lund, C.; Stephan, D. W. *Organometallics* **2013**, *32*, 4730−4732.

(44) For an experimental study investigating the σ-donor ability of NHC vs phosphine ligands, see: Diez-Gonzalez, S.; Nolan, S. P. *J. Coord. Chem. Rev.* **2007**, *251*, 874−883.

(45) Donation through the π-face of NHCs (via mesityl groups) has been proposed to stabilize the high oxidation state metallacyclobutane (+IV, d^4). For the effect of π-face donation on redox potentials, see: (a) Leuthäusser, S.; Schmidts, V.; Thiele, C. M.; Plenio, H. *Chem.—Eur. J.* **2008**, *14*, 5465−5481. (b) Credendino, R.; Falivene, L.; Cavallo, L. *J. Am. Chem. Soc.* **2012**, *134*, 8127−8135.
(46) For the effect of NHC vs phosphine ligands on the oxidation potential of Ru complexes, see: Getty, K.; Delgado-Jaime, M. U.; Kennepohl, P. *J. Am. Chem. Soc.* **2007**, *129*, 15774−15776.
(47) For attempts to achieve *Z* selectivity through modification of monodentate NHC ligands, see: (a) Vehlow, K.; Maechling, S.; Blechert, S. *Organometallics* **2006**, *25*, 25−28. (b) Ledoux, N.; Linden, A.; Allaert, B.; Mierde, H. V.; Verpoort, F. *Adv. Synth. Catal.* **2007**, *349*, 1692−1700. (c) Vougioukalakis, G. C.; Grubbs, R. H. *J. Am. Chem. Soc.* **2008**, *130*, 2234−2245. (d) Anderson, D. R.; Ung, T.; Mkrtumyan, G.; Bertrand, G.; Grubbs, R. H.; Schrodi, Y. *Organometallics* **2008**, *27*, 563−566. (e) Rosen, E. L.; Sung, D. H.; Chen, Z.; Lynch, V. M.; Bielawski, C. W. *Organometallics* **2010**, *29*, 250−256. (f) Peeck, L. H.; Leuthäusser, S.; Plenio, H. *Organometallics* **2010**, *29*, 4339−4345.
(48) For a computational study on the control of *E*/*Z* selectivity in dichloride systmes, see: Bahri-Laleh, N.; Credendino, R.; Cavallo, L. *Beilstein J. Org. Chem.* **2011**, *7*, 40−45.
(49) (a) Khan, R. K. M.; Torker, S.; Hoveyda, A. H. *J. Am. Chem. Soc.* **2013**, *135*, 10258−10261. (b) Koh, M. J.; Khan, R. K. M.; Torker, S.; Hoveyda, A. H. *Angew. Chem., Int. Ed.* **2014**, *53*, 1968−1972.
(50) For a theoretical study of the influence of anionic ligands in Mo, W, and Re systems on the barrier of olefin coordination and mcb stability, see: (a) Solans-Monfort, X.; Clot, E.; Coperet, C.; Eisenstein, O. *J. Am. Chem. Soc.* **2005**, *127*, 14015−14025. (b) Poater, A.; Solans-Monfort, X.; Clot, E.; Coperet, C.; Eisenstein, O. *J. Am. Chem. Soc.* **2007**, *129*, 8207−8216.
(51) Sanford, M. S.; Henling, L. M.; Day, M. W.; Grubbs, R. H. *Angew. Chem., Int. Ed.* **2000**, *39*, 3451−3453.
(52) Zhao, Y.; Truhlar, D. G. *Acc. Chem. Res.* **2008**, *41*, 157−167.
(53) For a detailed analysis of frontier Kohn−Sham orbitals of the d^6 14e complexes $\mathbf{14e1_X}$ and the d^4 metallacyclobutanes $\mathbf{mcb_X}$ and the influence of anionic ligands, see the Supporting Information.
(54) Due to the absence of an electronic barrier for olefin association ($\mathbf{14e1_X} \rightarrow \mathbf{pc1_X}$) in the gas phase with dispersion corrected functionals (e.g., M06-L vs BP86), we have approximated the free energy ts for propene association (see dotted line in Figure 10), for which the loss of translational entropy (∼11−12 kcal/mol in gas phase) from the structures in $\mathbf{14e1_X}$ (that is, 14e complex + propene) is the main contribution. Since the ts for substrate dissociation in the absence of significant structural reorganization is likely characterized by a higher degree of rotational and vibrational freedom (vs **ts1**), the ts for propene dissociation ($\mathbf{pc1_X} \rightarrow \mathbf{14e1_X}$) will likely benefit to a larger extent from stabilization on the free energy surface (relative to **ts1**). Nonetheless, the relative free energy barriers for the $\mathbf{pc1_X} \rightarrow \mathbf{14e1_X}$ step reflect the enthalpic contributions for the pathways shown in Figure 9.
(55) The Ru=C bond increases from 1.831 Å in $\mathbf{14e1_{OMe}}$ to 1.855 Å in $\mathbf{pc1_{OMe}}$ (BP86/basis1). In the dichloride complex the corresponding bond lengths are 1.816 and 1.839 Å.
(56) An increase in MeO−Ru−OMe angle can also be attributed to the minimization of dipole moment, due to the increase of negative charge on the anions.
(57) Hoye, T. R.; Zhao, H. *Org. Lett.* **1999**, *1*, 1123−1125.
(58) Forman, G. S.; McConnell, A. E.; Tooze, R. P.; van Rensburg, W. J.; Meyer, W. H.; Kirk, M. M.; Dwyer, C. L.; Serfontein, D. W. *Organometallics* **2005**, *24*, 4528−4542.
(59) Adjiman, C. S.; Clark, A. J.; Cooper, G.; Taylor, P. C. *Chem. Commun.* **2008**, 2806−2808.
(60) Hoveyda, A. H.; Lombardi, P. J.; O'Brien, R. V.; Zhugralin, A. R. *J. Am. Chem. Soc.* **2009**, *131*, 8378−8379.
(61) (a) Imahori, T.; Ojima, H.; Yoshimura, Y.; Takahata, H. *Chem.—Eur. J.* **2008**, *14*, 10762−10771. (b) Schmidt, B.; Staude, L. *J. Org. Chem.* **2009**, *74*, 9237−9240. (c) Fuwa, H.; Saito, A.; Sasaki, M. *Angew. Chem., Int. Ed.* **2010**, *49*, 3041−3044. (d) Donohoe, T. J.; Race, N. J.; Bower, J. F.; Callens, C. K. A. *Org. Lett.* **2010**, *12*, 4094−4097. (e) Donohoe, T. J.; Bower, J. F. *Proc. Natl. Acad. Sci.* **2010**, *107*, 3373−3376. (f) Fuwa, H.; Yamaguchi, H.; Sasaki, M. *Tetrahedron* **2010**, *66*, 7492−7503. (g) Fuwa, H.; Kawakami, M.; Noto, K.; Muto, T.; Suga, Y.; Konoki, K.; Yotsu-Yamashita, M.; Sasaki, M. *Chem.—Eur. J.* **2013**, *19*, 8100−8110.
(62) For computational studies indicating the preference for anti- vs syn-to-NHC pathway and the stabilizing effect of a polar medium on the latter, see: (a) Correa, A.; Cavallo, L. *J. Am. Chem. Soc.* **2006**, *128*, 13352−13353. (b) Benitez, D.; Tkatchouk, E.; Goddard, W. A., III *Chem. Commun.* **2008**, 6194−6196.
(63) For the experimental evidence regarding an olefin complex trans to a neutral donor (phosphine) ligand, see: (a) Tallarico, J. A.; Bonitatebus, P. J.; Snapper, M. L. *J. Am. Chem. Soc.* **1997**, *119*, 7157−7158. For related examples corresponding to olefin complexes syn to the NHC ligand, see: (b) Trnka, T. M.; Day, M. W.; Grubbs, R. H. *Organometallics* **2001**, *20*, 3845−3847. (c) Anderson, D. R.; Hickstein, D. D.; O'Leary, D. J.; Grubbs, R. H. *J. Am. Chem. Soc.* **2006**, *128*, 8386−8387. For related computational studies on olefin complexes, see: (d) Benitez, D.; Tkatchouk, E.; Goddard, W. A., III *Organometallics* **2009**, *28*, 2643−2645. (e) Stewart, I. C.; Benitez, D.; O'Leary, D. J.; Tkatchouk, E.; Day, M. W.; Goddard, W. A., III; Grubbs, R. H. *J. Am. Chem. Soc.* **2009**, *131*, 1931−1938.
(64) For a representative list of Ru carbene complexes, wherein the cis orientation between anionic ligands is imposed due to geometric constraints, see: (a) Hansen, S. M.; Rominger, F.; Metz, M.; Hofmann, P. *Chem.—Eur. J.* **1999**, *5*, 557−566. (b) Hansen, S. M.; Volland, M. A. O.; Rominger, F.; Eisenträger, F.; Hofmann, P. *Angew. Chem., Int. Ed.* **1999**, *38*, 1273−1276. (c) Monfette, S.; Fogg, D. E. *Organometallics* **2006**, *25*, 1940−1944. (d) Monfette, S.; Camm, K. D.; Gorelsky, S. I.; Fogg, D. E. *Organometallics* **2009**, *28*, 944−946.
(65) In a related Ru dithiolate complex (see ref 43b) with a larger linker between the two sulfur anions the S−Ru−S angle is 147.4°, which allows both sulfur atoms to be coordinated syn to the NHC ligand.
(66) There is likely a more severe degree of steric interaction between the adamantyl ligand and the metallacyclobutane in **VII** (see ref 10c). Furthermore, stabilizing back bonding ($d_{xz}/d_{yz} \rightarrow$ NHC) is only feasible in **VIII**, wherein the heterocyclic moiety occupies the axial position (*z* direction) of the d^4 mcb.

NOTE ADDED AFTER ASAP PUBLICATION

Schemes 8 and 9 and ref 54 contained errors in the version published ASAP February 17, 2014; the correct version reposted February 20, 2014.